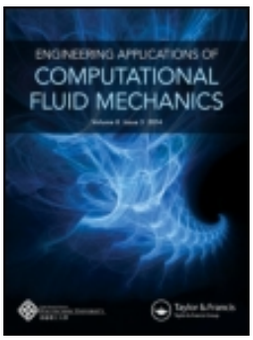

Taylor & Francis
Taylor & Francis Group

Engineering Applications of Computational Fluid Mechanics

ISSN: 1994-2060 (Print) 1997-003X (Online) Journal homepage: http://www.tandfonline.com/loi/tcfm20

A cost-effective FE method for 2D Navier–Stokes equations

A. C. Kengni Jotsa & V. A. Pennati

To cite this article: A. C. Kengni Jotsa & V. A. Pennati (2015) A cost-effective FE method for 2D Navier–Stokes equations, Engineering Applications of Computational Fluid Mechanics, 9:1, 66-83, DOI: 10.1080/19942060.2015.1004811

To link to this article: http://dx.doi.org/10.1080/19942060.2015.1004811

Engineering Applications of Computational Fluid Mechanics, 2015
Vol. 9, No. 1, 66–83, http://dx.doi.org/10.1080/19942060.2015.1004811

Taylor & Francis
Taylor & Francis Group

A cost-effective FE method for 2D Navier–Stokes equations

A. C. Kengni Jotsa[a] and V. A. Pennati[b]*

[a]*African Institute For Mathematical Sciences (AIMS-Cameroon), PO Box 608 Limbe Crystal Gardens, South West Region;* [b]*Università Degli Studi dell'Insubria, Dipartimento Di Scienza e Alta Tecnologia, Via Valleggio 11, 22100 Como, Italy*

(*Received 22 October 2013; final version received 11 September 2014*)

A cost-effective approach to the solution of 2D Navier–Stokes equations for incompressible fluid flow problems is presented. The aim is to reach a good compromise between numerical properties and computational efficiency. In order to achieve the set goal, the nonlinear convective terms are approximated by means of characteristics and spatial approximations of equal order are performed by polynomials of degree two. In this way, the computational kernels are reduced to elliptic ones for which solution very efficient techniques are available. The time-advancing is afforded by a fractional step method combined with a stabilization technique suitably simplified, so that the inf-sup condition is easily overcome. The algebraic systems generated by the new technique are solved by an iterative solver (Bi-CGSTAB), preconditioned by means of a suitable Schwarz additive scalable preconditioner. The properties of the new method have been confirmed from the comparison among the results obtained by it, and those obtained from other methods in the solution of some well known test problems. The obtained results, both in terms of accuracy and computational efficiency, make realistic the possibility to extend the method to 3D problems and to develop a multidomain approach.

Keywords: 2D Navier–Stokes; fractional step; finite element; stabilization; Schwarz preconditioner

1. Introduction

Nowadays in fluid dynamics, the transient incompressible Navier–Stokes equations are widely accepted as a mathematical model for the description of incompressible viscous flows. Their application to the solution of real problems, both 2D and 3D, is more and more widespread and requires a great computing effort, see for example (Cavazzutti, Corticelli, Masina, & Saponelli, 2013; Kumar, Kumar, & Kumar Das, 2009; Stickland, Fabre, Scanlon, Oldroyd, Mickelson, & Astrup, 2013). The system of equations is made up of the momentum equations and the incompressibility relation, and it is well known that the main difficulties in its solution reside in the approximation of the convective term and in the calculation of the pressure. A large amount of numerical methods have been developed particularly in the framework of finite elements (FE) (Baker, Dougalis, & Karakashian, 1982; Choi, Choi, & Yoo, 1997; Codina & Soto, 2004; Plana Fattori, Chantoiseau, Doursat, & Flick, 2013; Sun, Zhang, & Ren, 2012), of cell-centred finite volumes (Deponti, Pennati, & De Biase, 2006; Deponti, & Pennati, et al., 2006; Feraudi & Pennati, 1997; Kim & Moin, 1985; Pai, Prakash, & Patnaik, 2013) or cell-vertex finite volumes (Hookey & Baliga, 1998; Malan, Lewis, & Nithiarasu, 2002; Tritthart & Gutknecht, 2007; Vrahliotis, Pappou, & Tsangaris, 2012) and finite differences (Ali, Fieldhouse, & Talbot, 2011; Kumar, Dass, & Dewan, 2010; Shih & Tan, 1989). In the finite difference (FD) and finite volume (FV) schemes some methods for time-advancing are based on the so-called SIMPLE method, and its developments (for example, SIMPLER, SIMPLEC, SIMPLEX, PISO, etc.). The SIMPLE method (Patankar, 1980) can be regarded as quite a rough (but simple) preconditioner obtained by an approximation of the upper triangular matrix **U** (usually the principal diagonal) of the **LU** factorization of the global system matrix. Two important drawbacks are inherent the SIMPLE preconditioner, namely: the low rate of convergence and the global approach to the solution of the system of equations (particularly computationally heavy in 3D problems) (Acharya & Moukallad, 1989; Van Doormal & Raithby, 1984). In order to improve the computational efficiency of the solvers used in FD and FV approximations, a huge literature has been developed regarding the multigrid methods. These can be very efficiently formulated if based on structured grids (the so called geometric multigrids), because the spectral analysis of the stiffness matrices allow us to choose optimal smoothers (Donatelli, Molteni, Pennati, & Serra Capizzano, In press). A potential drawback of the geometric multigrid solvers is their difficulty to solve problems defined in general domains, in fact, in this case a transformation from the physical space to the computational one has to be performed (Kumar et al., 2010). Another important point involved in the time-advancing is the approximation of the convective term. It is nonlinear, and for its approximation several techniques have been developed, for example, the implicit one (based

*Corresponding author. Email: VPennati@teletu.it

on a Newton cycle requiring at every iteration the solution of a linear system), the semi implicit one (in which the nonlinear term is approximated explicitly) and the Picard approximation (in which the transferring term is "frozen" at time n and the gradient of velocity at time $n+1$). The first approximation is of second order but very heavy with respect to the computing time, the second one requires a severe restriction on Δt in order to guarantee the stability, the third one is only first order in time. In transient problems, besides the schemes commonly used for advancing in time, there is another approach called the fractional steps; it is based on the splitting of the differential operator in the sum of two suitable differential operators. This last technique combined with a Lagrangian approximation of the convective term is the base of our time-marching scheme.

In this paper, a numerical approach for the solution of 2D incompressible Navier–Stokes equations is presented with the aim of obtaining an accurate solution while maintaining a low computational effort. This choice is very important because we are interested in generalizing the presented method to problems with moving boundaries (in particular to 3D problems). The new method can be considered optimal in the sense that its formulation attempts to obtain a good compromise between numerical properties (accuracy and stability) and computational efficiency. The main features of the method are: using a triangular (curved edges) FE spatial approximation with polynomials of degree two for velocity and pressure (and temperature); time-advancing by a fractional step approach in which the nonlinear convective term is approximated by characteristics and the pressure correction is calculated by solving a Poisson equation (Codina & Badia, 2006; Gervasio & Saleri, 2006; Han, Zhou, & Tu, 2013; Shirokoff & Rosales, 2011); addition of a suitable stabilization technique in order to overcome the instabilities inherent in the equal-order choice. A well-known technique of stabilization is the one based on the definition of subscale velocities formulated by Codina and Soto (2004). Unfortunately, this technique depends on a weight parameter τ whose estimation generally is not easy. In section 4, a very simple rule for calculating the τ value is suggested and its efficiency verified by solving several numerical tests. In the new technique the most expensive computational kernels are reduced to elliptic ones so that, in order to reduce as much as possible the computational effort, an iterative method (Bi-CGSTAB) preconditioned by an additive Schwarz preconditioner is used. Such preconditioners are endowed with very interesting properties, in particular the scalability and the computational flexibility. The latter is dependent on the number of subdomains in which the domain is divided, and on the level of *fill-in* chosen for the incomplete **LU** factorization of the local stiffness matrix. The multidomain approach, besides being a necessary tool for creating an efficient Schwarz preconditioner, could be also considered a convenient starting point for developing distributed memory parallel computing algorithms (Corti & Pennati, 1997).

The content of the paper is organized as follows. Section 2 introduces the governing equations completed by the energy equation. Section 3 describes the time-advancing to be used. In Section 4, the issue of the approximation of the 2D Navier–Stokes equations with stabilization is considered. The main result of this section consists of the fractional step scheme (58)–(63) that has been implemented in our in-house code. Finally, in Section 5 the flexibility and the efficiency of the method are illustrated by four examples: the two dimensional unsteady flow of decaying vortices, two lid-driven problems: the first one with analytical solution and the second one with constant boundary condition and, finally, some thermal convection problems in a square cavity. The last section is devoted to some concluding remarks.

2. Governing equations

Let Ω be a bounded domain of $\mathbb{R}^2$ occupied by the fluid, with Lipschitz boundary $\partial\Omega$ and $[0, T]$ the time interval of analysis. The 2D Navier–Stokes problem for incompressible flows consists in finding a velocity $\boldsymbol{u}$, a pressure p, and a temperature T such that:

$$\frac{\partial \boldsymbol{u}}{\partial t} + \boldsymbol{u}\cdot\nabla\boldsymbol{u} - \nu\Delta\boldsymbol{u} + \nabla p = \boldsymbol{f} \text{ in } \Omega, \quad t \in (0,T) \tag{1}$$

$$\nabla\cdot\boldsymbol{u} = 0 \text{ in } \Omega, \quad t \in (0,T) \tag{2}$$

$$\boldsymbol{u} = 0 \text{ on } \partial\Omega, \quad t \in (0,T) \tag{3}$$

$$\boldsymbol{u}|_{t=0} = \boldsymbol{u_0} \text{ in } \Omega \tag{4}$$

$$\frac{\partial \mathrm{T}}{\partial t} + \boldsymbol{u}\cdot\nabla\mathrm{T} - \Gamma\Delta\mathrm{T} = \boldsymbol{S} \text{ in } \Omega, t \in (0,T) \tag{5}$$

$$\mathrm{T} = 0 \text{ on } \partial\Omega, \quad t \in (0,T) \tag{6}$$

$$\mathrm{T}|_{t=0} = \mathrm{T}_0 \text{ in } \Omega \tag{7}$$

where $\boldsymbol{f}$ denotes a volumetric body force such as gravitation, ν the kinematic viscosity, $\boldsymbol{u_0}$ and T_0 the initial velocity and temperature respectively. We have considered homogeneous Dirichlet boundary conditions (3) and (6) for simplicity. We need to introduce some useful notations, e.g., to denote by $\mathrm{H}^1(\Omega)$ the Sobolev space of functions whose first derivatives belong to $\mathrm{L}^2(\Omega)$, and by $\mathrm{H}^1_0(\Omega)$ the subspace of $\mathrm{H}^1(\Omega)$ of functions with zero trace on $\partial\Omega$.

3. Time-advancing scheme

As the nonlinear convective term of the momentum equation (1) needs to be treated with care, and as we would like to reduce the computational effort significantly, we use the second-order characteristics scheme (Pironneau, 1982) that computes the values of the variable of interest at the foot of the trajectory. In fact, assume for instance we have

the equation:

$$\frac{DQ}{Dt} = \Psi \tag{8}$$

where $\frac{DQ}{Dt}$ represents the total derivative, that is $\frac{\partial Q}{\partial t} + \boldsymbol{u} \cdot \nabla Q = \Psi$ with $\boldsymbol{u}$ known velocity.

If the total derivative is approximated with a backward Euler scheme:

$$\frac{DQ}{Dt} \cong \frac{Q^{n+1}(\mathbf{x}) - Q^n_{ft}}{\Delta t} \tag{9}$$

then an implicit semi-Lagrangian scheme for (8) is:

$$\frac{Q^{n+1}(\mathbf{x}) - Q^n_{ft}}{\Delta t} = \Psi^{n+1}(\mathbf{x}) \tag{10}$$

Knowing the velocity field $\boldsymbol{u}$, the foot of trajectory can be calculated by:

$$\tilde{\boldsymbol{x}}_{ft} = \mathbf{x} - \Delta t \boldsymbol{u}^{n+1}(\mathbf{x}) \tag{11}$$

The index *ft* shows that the relevant variable is calculated (at instant t^n) at the foot of a trajectory associated to the velocity field $\boldsymbol{u}$. Being given $\mathbf{x} \in \Omega$ and $\lambda \in [0, T]$, the trajectories are the functions $\tilde{\boldsymbol{X}}(t; \lambda, \mathbf{x})$ such that:

$$\frac{d\tilde{\boldsymbol{X}}(t;\lambda,\mathbf{x})}{dt} = \boldsymbol{u}(t;\ \tilde{\boldsymbol{X}}(t;\lambda,\ \mathbf{x})) \tag{12}$$

$$\tilde{\boldsymbol{X}}(\lambda;\ \lambda,\ \mathbf{x}) = \mathbf{x} \tag{13}$$

The application of a similar approach to a convective-diffusive equation gives:

$$\frac{\mathrm{T}^{n+1}(\mathbf{x}) - \mathrm{T}^n(\tilde{\boldsymbol{x}}_{ft})}{\Delta t} - \Gamma \Delta \mathrm{T}^{n+1}(\mathbf{x}) = S^{n+1}(\mathbf{x}) \tag{14}$$

where Γ is the diffusion parameter and S a source term. Of course, also a second-order approximation in time could be used for equation (14), but in order to reduce the computational effort we decided to use a first-order approximation. The interpolation of T^n is easily calculated after having located the element to which the foot $\tilde{\boldsymbol{x}}_{ft}$ belongs.The generalization of the above technique to the momentum equation is direct and reads (vectorially):

$$\boldsymbol{u}^{n+1} - \Delta t \nu \Delta \boldsymbol{u}^{n+1} = \boldsymbol{u}^n(\tilde{\boldsymbol{x}}_{ft}) + \Delta t\,(-\nabla p^n + \boldsymbol{f}^{n+1}) \tag{15}$$

In (15) it can be seen that the gradient of pressure is evaluated at the instant n, therefore considering instead of $\boldsymbol{u}^{n+1}$ a provisional velocity $\tilde{\boldsymbol{u}}^{n+\frac{1}{2}}$, applying to it the divergence operator and considering the incompressibility relation, we can write a Poisson equation for the pressure correction $\tilde{p}^{n+1}$:

$$-\Delta \tilde{p}^{n+1} = -\frac{1}{\Delta t} \nabla \cdot \tilde{\boldsymbol{u}}^{n+\frac{1}{2}} \tag{16}$$

Finally the adjourned values of velocity and pressure are given by:

$$\boldsymbol{u}^{n+1} = \tilde{\boldsymbol{u}}^{n+\frac{1}{2}} - \Delta t \Delta \tilde{p}^{n+1} \tag{17}$$

$$p^{n+1} = p^n + \tilde{p}^{n+1} \tag{18}$$

The following important remarks can be made:

a) the difficulties inherent in the nonlinearity of the convective term are overcome, infact, the stability is granted under mild conditions (characteristics are unconditionally stable for linear problems);
b) the incompressibility is granted by construction;
c) the most expensive computational kernels stem from elliptic problems.

4. Approximation of the 2D Navier–Stokes equations with stabilization

In order to obtain a weak formulation of problem (1) – (4), we formally multiply (1) by a suitable function $\boldsymbol{\psi}$ and by integration in Ω we obtain:

$$\int_\Omega \frac{\partial \boldsymbol{u}}{\partial t} \cdot \boldsymbol{\psi}\, d\Omega + \int_\Omega [(\boldsymbol{u} \cdot \nabla)\boldsymbol{u}] \cdot \boldsymbol{\psi}\, d\Omega - \nu \int_\Omega \Delta \boldsymbol{u} \cdot \boldsymbol{\psi}\, d\Omega + \int_\Omega \nabla p \cdot \boldsymbol{\psi}\, d\Omega = \int_\Omega \boldsymbol{f} \cdot \boldsymbol{\psi}\, d\Omega \tag{19}$$

Using the Green formula we have:

$$-\nu \int_\Omega \Delta \boldsymbol{u} \cdot \boldsymbol{\psi}\, \mathrm{d}\Omega = \nu \int_\Omega \nabla \boldsymbol{u} \cdot \nabla \boldsymbol{\psi} \mathrm{d}\Omega - \nu \int_{\partial\Omega} \frac{\partial \boldsymbol{u}}{\partial \boldsymbol{n}} . \boldsymbol{\psi} d\gamma \tag{20}$$

$$\int_\Omega \nabla p \cdot \boldsymbol{\psi}\, d\Omega = -\int_\Omega p \nabla \cdot \boldsymbol{\psi}\, d\Omega + \int_{\partial\Omega} p \boldsymbol{\psi} \cdot \boldsymbol{n}\, d\gamma \tag{21}$$

Keeping into account the homogeneous boundary conditions, and by substitution of the last two relations in the momentum equation, we obtain:

$$\int_\Omega \frac{\partial \boldsymbol{u}}{\partial t} \cdot \boldsymbol{\psi}\, d\Omega + \int_\Omega [(\boldsymbol{u} \cdot \nabla)\boldsymbol{u}] \cdot \boldsymbol{\psi}\, d\Omega + \nu \int_\Omega \nabla \boldsymbol{u} \cdot \nabla \boldsymbol{\psi}\, d\Omega - \int_\Omega p\ \nabla \cdot \boldsymbol{\psi}\, d\Omega = \int_\Omega \boldsymbol{f} \cdot \boldsymbol{\psi}\, d\Omega + \int_{\partial\Omega} \left(\nu \frac{\partial \boldsymbol{u}}{\partial \boldsymbol{n}} - p\boldsymbol{n} \right) \cdot \boldsymbol{\psi}\, d\gamma \qquad \forall\, \boldsymbol{\psi} \epsilon \mathbf{V} \tag{22}$$

By multiplying (2) by a suitable test function $\varphi \in Q$, we obtain:

$$\int_\Omega \varphi\ \nabla \cdot \boldsymbol{u}\, d\Omega = 0 \qquad \forall\, \varphi \in Q \tag{23}$$

The spaces $\mathbf{V}$ and Q can be chosen $\mathbf{V} := [\mathrm{H}^1_0(\Omega)]^2$ and $Q := \mathrm{L}^2(\Omega)$, respectively.

Equations (22) and (23) are the weak vectorial forms of the equations that we are interested in solving. Rewriting the fractional step (15)–(18) with respect to each component of the velocity field $\boldsymbol{u} = (u, v)$ and applying the weak formulation to the velocity correction, the problem becomes:

to find $\boldsymbol{u}^{n+1} = (u^{n+1}, v^{n+1}) \in \mathrm{L}^2(\mathbb{R}^+; [\mathrm{H}^1(\Omega)]^2) \cap \mathrm{C}^0(\mathbb{R}^+; [\mathrm{L}^2(\Omega)]^2)$ and $p^{n+1} \in \mathrm{L}^2(\mathbb{R}^+; \mathrm{H}^1(\Omega))$ such that:

$$\frac{1}{\Delta t}\int_\Omega \tilde{u}^{n+\frac{1}{2}}\psi_1 d\Omega + \nu\int_\Omega \nabla\tilde{u}^{n+\frac{1}{2}}\cdot\nabla\psi_1 d\Omega = -\int_\Omega \frac{\partial p^n}{\partial x}\psi_1 d\Omega + \int_\Omega f_u^{n+1}\psi_1\, d\Omega + \frac{1}{\Delta t}\int_\Omega u^n(\tilde{\boldsymbol{x}}_{ft})\psi_1\, d\Omega \quad \forall\, \psi_1 \in V_1 \tag{24}$$

$$\frac{1}{\Delta t}\int_\Omega \tilde{v}^{n+\frac{1}{2}}\psi_2 d\Omega + \nu\int_\Omega \nabla\,\tilde{v}^{n+\frac{1}{2}}\cdot\nabla\psi_2 d\Omega = -\int_\Omega \frac{\partial p^n}{\partial y}\psi_2\, d\Omega + \int_\Omega f_v^{n+1}\psi_2\, d\Omega + \frac{1}{\Delta t}\int_\Omega v^n(\tilde{\boldsymbol{x}}_{ft})\psi_2 d\Omega \quad \forall\psi_2 \in V_2 \tag{25}$$

$$\int_\Omega \nabla\tilde{p}^{n+1}\cdot\nabla\varphi d\Omega = -\frac{1}{\Delta t}\int_\Omega\left(\frac{\partial\tilde{u}^{n+\frac{1}{2}}}{\partial x} + \frac{\partial\tilde{v}^{n+\frac{1}{2}}}{\partial y}\right)\varphi\, d\Omega \quad \forall\,\varphi \in Q \tag{26}$$

$$p^{n+1} = p^n + \tilde{p}^{n+1} \tag{27}$$

$$\int_\Omega u^{n+1}\varphi\, d\Omega = \int_\Omega \tilde{u}^{n+\frac{1}{2}}\varphi\, d\Omega - \Delta t\int_\Omega \frac{\partial\tilde{p}^{n+1}}{\partial x}\varphi\, d\Omega \quad \forall\,\varphi \in Q \tag{28}$$

$$\int_\Omega v^{n+1}\varphi\, d\Omega = \int_\Omega \tilde{v}^{n+\frac{1}{2}}\varphi\, d\Omega - \Delta t\int_\Omega \frac{\partial\tilde{p}^{n+1}}{\partial y}\varphi\, d\Omega \quad \forall\,\varphi \in Q \tag{29}$$

Let $T_h = \{K\}$ be a suitable triangulation of the domain Ω. By using equal-order velocity-pressure approximation (i.e., $\psi_1 = \psi_2 = \varphi \in \mathrm{X}_h^2$) the system of equations (24)–(29) can be rewritten as follow:

$$\sum_K\left[\frac{1}{\Delta t}\sum_i \tilde{u}_i^{n+\frac{1}{2}}\int_K \varphi_i\varphi_j dK + \nu\sum_i \tilde{u}_i^{n+\frac{1}{2}}\int_K \nabla\varphi_i\cdot\nabla\varphi_j dK\right] = \sum_K\left[-\sum_i p_i^n\int_K\frac{\partial\varphi_i}{\partial x}\varphi_j dK + \sum_i (f_i^{n+1})_u\int_K\varphi_i\varphi_j dK + \frac{1}{\Delta t}\sum_i u_i^n(\tilde{\boldsymbol{x}}_{ft})\int_K\varphi_i\varphi_j dK\right] \tag{30}$$

$$\sum_K\left[\frac{1}{\Delta t}\sum_i \tilde{v}_i^{n+\frac{1}{2}}\int_K \varphi_i\varphi_j dK + \nu\sum_i \tilde{v}_i^{n+\frac{1}{2}}\int_K \nabla\varphi_i\cdot\nabla\varphi_j dK\right] = \sum_K\left[-\sum_i p_i^n\int_K\frac{\partial\varphi_i}{\partial y}\varphi_j dK + \sum_i (f_i^{n+1})_v\int_K\varphi_i\varphi_j dK + \frac{1}{\Delta t}\sum_i v_i^n(\tilde{\boldsymbol{x}}_{ft})\int_K\varphi_i\varphi_j dK\right] \tag{31}$$

$$\sum_K\left[\sum_i \tilde{p}_i^{n+1}\int_K\nabla\varphi_i\cdot\nabla\varphi_j\, dK\right] = -\frac{1}{\Delta t}\sum_K\left[\sum_i \tilde{u}_i^{n+\frac{1}{2}}\int_K\frac{\partial\varphi_i}{\partial x}\varphi_j dK + \sum_i \tilde{v}_i^{n+\frac{1}{2}}\int_K\frac{\partial\varphi_i}{\partial y}\varphi_j dK\right] \tag{32}$$

$$p_i^{n+1} = p_i^n + \tilde{p}_i^{n+1} \tag{33}$$

$$\sum_K\left[\sum_i u_i^{n+1}\int_K\varphi_i\varphi_j\, dK\right] = \sum_K\left[\sum_i \tilde{u}_i^{n+\frac{1}{2}}\int_K\varphi_i\varphi_j dK - \Delta t\sum_i\tilde{p}_i^{n+1}\int_K\frac{\partial\varphi_i}{\partial x}\varphi_j dK\right] \tag{34}$$

$$\sum_K\left[\sum_i v_i^{n+1}\int_K\varphi_i\varphi_j\, dK\right] = \sum_K\left[\sum_i \tilde{v}_i^{n+\frac{1}{2}}\int_K\varphi_i\varphi_j dK - \Delta t\sum_i\tilde{p}_i^{n+1}\int_K\frac{\partial\varphi_i}{\partial y}\varphi_j dK\right] \tag{35}$$

The algebraic form of equations (30)–(35) is:

$$\frac{1}{\Delta t}\mathbf{M}\tilde{\boldsymbol{u}}^{n+\frac{1}{2}} + \nu\mathbf{A}\tilde{\boldsymbol{u}}^{n+\frac{1}{2}} = -\mathbf{B}^T\boldsymbol{p}^n + \mathbf{M}\boldsymbol{f}_u^{n+1} + \frac{1}{\Delta t}\mathbf{M}\boldsymbol{u}^n(\tilde{\boldsymbol{x}}_{ft}) \tag{36}$$

$$\frac{1}{\Delta t}\mathbf{M}\tilde{\boldsymbol{v}}^{n+\frac{1}{2}} + \nu\mathbf{A}\tilde{\boldsymbol{v}}^{n+\frac{1}{2}} = -\mathbf{C}^T\boldsymbol{p}^n + \mathbf{M}\boldsymbol{f}_v^{n+1} + \frac{1}{\Delta t}\mathbf{M}\boldsymbol{v}^n(\tilde{\boldsymbol{x}}_{ft}) \tag{37}$$

$$\mathbf{A}\tilde{\boldsymbol{p}}^{n+1} = -\frac{1}{\Delta t}\left[\mathbf{B}^T\tilde{\boldsymbol{u}}^{n+\frac{1}{2}} + \mathbf{C}^T\tilde{\boldsymbol{v}}^{n+\frac{1}{2}}\right] \tag{38}$$

$$\boldsymbol{p}^{n+1} = \boldsymbol{p}^n + \tilde{\boldsymbol{p}}^{n+1} \tag{39}$$

$$\mathbf{M}\boldsymbol{u}^{n+1} = \mathbf{M}\tilde{\boldsymbol{u}}^{n+\frac{1}{2}} - \Delta t\,\mathbf{B}^{\mathrm{T}}\tilde{\boldsymbol{p}}^{n+1} \tag{40}$$

$$\mathbf{M}\boldsymbol{v}^{n+1} = \mathbf{M}\tilde{\boldsymbol{v}}^{n+\frac{1}{2}} - \Delta t\,\mathbf{C}^{\mathrm{T}}\tilde{\boldsymbol{p}}^{n+1} \tag{41}$$

where $\mathbf{A} = \sum_K\int_K\nabla\varphi_i\cdot\nabla\varphi_{\mathrm{j}}\mathrm{d}K$ is the stiffness matrix, $\mathbf{M} = \sum_K\int_K\varphi_i\varphi_j dK$ is the mass matrix, $\mathbf{B} = \sum_K\int_K\frac{\partial\varphi_i}{\partial x}\varphi_j dK$ is the matrix of the x-component of the gradient operator and $\mathbf{C} = \sum_K\int_K\frac{\partial\varphi_i}{\partial y}\varphi_j dK$ is the matrix of the y-component of the gradient operator.

Remark 1. It is easy to see that all the algebraic systems of (36)–(41) are reduced to elliptic-like ones so that they are optimal from a computational point of view, in particular the solutions can be calculated by an iterative method preconditioned by a Schwarz scalable additive preconditioner.

Remark 2. If the domain Ω does not change during the transient, the matrices to be built (just once) are **M, A, B, C.**

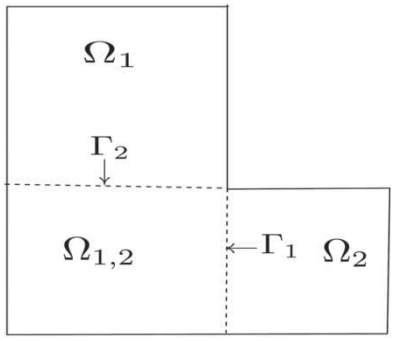

Figure 1. Example of overlapping subdivision with two subdomains.

Remark 3. In order to apply the Projection Method, the variables $\tilde{u}^{n+\frac{1}{2}}$, $\tilde{v}^{n+\frac{1}{2}}$ and $\tilde{p}^{\,n+1}$ have to belong to the spaces:

$$\tilde{u}^{n+\frac{1}{2}},\ \tilde{v}^{n+\frac{1}{2}} \ \epsilon \ \ \mathrm{H}_{0,\,div}$$
$$= \{\boldsymbol{u}^{\mathrm{n}+1}\epsilon[\mathrm{L}^2(\Omega)]^2 : \nabla\cdot\boldsymbol{u}^{n+1} = 0,\ \boldsymbol{u}^{\mathrm{n}+1}\cdot\boldsymbol{n} = 0 \text{ on } \partial\Omega\} \tag{42}$$

and $\tilde{p}^{n+1} \epsilon \mathrm{H}^1(\Omega)$

4.1. *Schwarz scalable additive preconditioner*

We give a brief description of the Schwarz preconditioner for elliptic problems introduced in Quarteroni and Valli (1999) and adopted in this paper. We consider, for example, the domain Ω as decomposed in two overlapping subdomains Ω_1 and Ω_2, see Figure 1, and we wish to solve the Poisson problem with homogeneous boundary conditions:

$$-\Delta u = f \ \text{ in } \Omega \tag{43}$$
$$u \ = \ 0 \ \text{ on } \partial\Omega \tag{44}$$

Let $\partial\Omega$, $\partial\Omega_1$, $\partial\Omega_2$ be the boundaries of Ω, Ω_1 , Ω_2 respectively, and Γ_1 , Γ_2 the internal boundaries of Ω_1 and Ω_2 respectively. Let u_{i}^k denote the approximate solution, after k iterations, on $\bar{\Omega}_i = \Omega_i \cup \partial\Omega_i$ with i = 1 and 2, and $u_1^k|\Gamma_2$ (respectively $u_2^k|\Gamma_1$) the restriction of u_1^k (respectively u_2^k) on Γ_2 (respectively Γ_1). Let u^0 an initial function defined in Ω and vanishing on $\partial\Omega$ and set $u_2^0 = u^0|\Omega_2$.Therefore, the Schwarz approach consists of defining two sequences u_1^{k+1} and u_2^{k+1} with $k \geq 0$ and solving iteratively the two boundary-value problems for u_1^{k+1} and u_2^{k+1} :

$$-\Delta u_1^{k+1} = f \ \text{ in } \Omega_1 \tag{45}$$
$$u_1^{k+1} = \ u_2^k \text{ on } \Gamma_1 \tag{46}$$
$$u_1^{k+1} = 0 \text{ on } \partial\Omega_1 \cup \partial\Omega \tag{47}$$

and

$$-\Delta u_2^{k+1} = f \ \text{ in } \Omega_2 \tag{48}$$
$$u_2^{k+1} = \ u_1^k \text{ on } \Gamma_2 \tag{49}$$
$$u_2^{k+1} = 0 \text{ on } \partial\Omega_2 \cup \partial\Omega \tag{50}$$

In order to define the variational formulation of the Schwarz problem at the discrete level, we set $\mathrm{V} := \mathrm{H}_0^1(\Omega)$,$\mathrm{V}_{\mathrm{i}}^0 := \mathrm{H}_0^1(\Omega_{\mathrm{i}})$. We define the finite element space:

$\mathrm{V_h} := \{\mathrm{v} \in \mathrm{V} : \mathrm{v}|_K \in \mathrm{P}r\,(K)\,, \forall K \in T_h\} \subset \mathrm{V} = \mathrm{H}_0^1(\Omega)$ where Pr are polynomials of degree $\leq r$. We know that a FE approximation to the original Poisson problem (43–44) consists in finding $u_h \in \mathrm{V}_h \subset \mathrm{V}$ such that:

$$a_h(u_h\ ,\ v_h) = \ (f\ ,\ v_h), \quad \forall\ v_h \ \in \ V_h \tag{51}$$

where $a_h(\cdot,)$ is the bilinear form given by:

$a_h(u_h\ ,\ \mathrm{v}_h) = \int_\Omega \nabla u_h\ .\ \nabla v_h\ \mathrm{d}\Omega$ and $(f\ , v_h)$ the linear form defined as $(f,\ v_h) = \int_\Omega f\ v_h d\Omega$. Then, the Schwarz method at the discrete level consists of assigning $u^0 \in \mathrm{V}_h$ and solving for each $k \geq 0$:

$$w_{1.h}^k \epsilon \mathrm{V}_{1,h}^0 :\ a_1(w_{1.h}^k, v_{1.h}) = \ (f, v_{1,h})_{\Omega_1} - \ a_1\ (u_h^k,\ v_{1,h})$$
$$\forall v_{1,h} \epsilon \ \mathrm{V}_{1,h}^0 \tag{52}$$
$$w_{2.h}^k \epsilon \mathrm{V}_{2,h}^0 :\ a_2(w_{2.h}^k, v_{2.h}) = \ (f, v_{2.h})_{\Omega_2} - \ a_2\ (u_h^k,\ v_{2,h})$$
$$\forall v_{2,h} \epsilon \ \mathrm{V}_{2,h}^0 \tag{53}$$
$$u_h^{k+1} = u_h^{k+1} + \ \widetilde{w_{1,h}^k} + \widetilde{w_{2,h}^k} \tag{54}$$

Where $\widetilde{w_{i,h}^k}$ is the function that extends $w_{i.h}^k$ by zeros in $\Omega\backslash\Omega_i$, $a_i\ (\cdot,\cdot)$ denotes the restriction of $a_h(\cdot,\cdot)$ to Ω_i and $\mathrm{V}_{i,h}^0 \subset \mathrm{V}_i^0$.

For the algebraic formulation of the Schwarz method we can think that the domain Ω is subdivided by M subdomains Ω_i with $i = 1, ..., M$. Let $\mathrm{V}_i^* = \{v \in \mathrm{V} : v = 0 \text{ in } \Omega\backslash\Omega_i\}$ and $\mathrm{V}_{i,h}^*$ be a finite dimensional subset of V_i^*. We define the prolongation operator $\mathbf{R}_i^T : \mathrm{V}_{i,h}^* \rightarrow \mathrm{V}_h$, which extends by zeros the degree of freedom outside Ω_{i}. The restriction operator $\mathbf{R}_{\mathrm{i}}$ is defined as the transposition of $\mathbf{R}_i^T$. By denoting $\mathbf{A_h}$ and $\mathbf{A_i}$ the stiffness matrices with respect to the global and local bilinear forms $a_h\ (\cdot,\ \cdot)$ and $a_i\ (\cdot,\ \cdot)$ and defining the operator $\mathbf{Q}_i$ like the matrix $\mathbf{Q}_i = \mathbf{R}_i^T\mathbf{A}_i^{-1}\mathbf{R}_i$, then after some algebraic manipulations the one level additive Schwarz iterative method reads for $M \geq 2$ subdomains:

$$\mathbf{u}_h^{k+1} = \ \mathbf{u}_h^k + \left(\sum_{i=1}^{M}\mathbf{Q}_i\right)(\mathbf{b}_h - \ \mathbf{A}_h\mathbf{u}_h^k), \quad k \geq 0 \tag{55}$$

where $k \geq 0$ is the index of iteration. Regarding (55) as a fixed-point relation, we can define the Schwarz method simply as a Richardson iterative method with preconditioner $\mathbf{P}_{as} = \left[\sum_{i=1}^{M}\mathbf{Q}_i\right]^{-1}$. Unfortunately, the convergence of the one level Schwarz method deteriorates when the number M of subdomains becomes larger because of the lack of information between subdomains Ω_i. In order to overcome this drawback, we have introduced a global coarse mesh as a particular subdomain Ω_0, so that

communications among all the subdomains are guaranteed. Therefore, the final form of the preconditioner is $\mathbf{P}_{asc}^{-1} = \left(\sum_{i=0}^{M} \mathbf{R}_i^T \mathbf{A}_i^{-1} \mathbf{R}_i\right)$. Since the final algebraic system (51) is $\mathbf{A_h u_h} = \mathbf{b_h}$, the preconditioned two level additive Schwarz system is written:

$$\mathbf{P}_{asc}^{-1}\mathbf{A}_h\,\mathbf{u}_h = \left(\sum_{i=0}^{M} \mathbf{R}_i^T \mathbf{A}_i^{-1} \mathbf{R}_i\right) \mathbf{A}_h \mathbf{u}_h = \left(\sum_{i=0}^{M} \mathbf{R}_i^T \mathbf{A}_i^{-1} \mathbf{R}_i\right) \mathbf{b}_h \tag{56}$$

A well-known theorem (Dryja & Widlund, 1989), under suitable conditions, provides a limit for the condition number $K(\mathbf{P}_{asc}^{-1}\mathbf{A}_h)$ of the Schwarz preconditioned matrix. Called h and H the diameters of the elements of the fine and coarse triangulations respectively, then we have:

$$K\ (\mathbf{P}_{asc}^{-1}\mathbf{A}_h) \leq c\left[1 + \frac{H}{h}\right]^2 \tag{57}$$

where c is a positive constant independent of H and h. Thus the presence of the coarse partition makes the convergence rate independent of both h and H. This property (scalability) is very desirable especially when the method is implemented on massively parallel architectures, and when the number of subdomains is big. We recall that the computational kernels of (36–41) are of elliptic kind so that a scalable Schwarz additive overlapping multidomains preconditioner is worthwhile to be adopted. The algorithm of the implementation of the Schwarz additive preconditioner can be seen in Kengni Jotsa (2012).

Remark 4. The number M of the subdomains in which Ω is divided, decides the efficiency of the Schwarz preconditioner. In fact, the number of nodes belonging to each subdomain depends on M and, of course, also on the subdomain form; both the choices should be as shrewd as possible in order to reach a good balance among the dimension of the local stiffness matrices $\mathbf{A}_i$ and the optimal computational time. Another choice influences the efficiency of the **P***as* and **P***asc* preconditioners, namely the level of *fill-in* allowed in the process of **LU** factorization to calculate the $\mathbf{A}_i^{-1}$ matrices, the so-called **I**ncomplete **LU** factorization (**ILU**) process.

4.2. The inf-sup condition and a stabilization

In a study (Guermond & Quartapelle, 1998) it is affirmed that the fractional step method based on the Poisson equation for pressure overcomes the inf-sup condition under a suitable limitation for Δt and for P_1 /P_1 linear approximation; without respecting the temporal limitation or for equal-order P_2 /P_2 approximation, the numerical solution is unstable. Since we are using equal-order P_2 /P_2 approximation, stabilization techniques needed in order to complete the formulation (36–41). Among the wide spread stabilized methods, we can quote the Galerkin least square technique (Franca & Hughes, 1993; Franca & Stenberg, 1991; Hughes, Franca, & Balestra, 1986), the least square method for first-order system such as (Bochev, Cai, Manteuffel, & McCormick, 1998) and the least square method for second-order scheme (Fortin & Boivin, 1990; Silvester & Kechkar, 1990) and other methods (Brezzi & Douglas, 1988; Douglas & Wang, 1989). Codina (2001; Codina & Soto (2004)) built a stabilization technique based on the definition of the "subscale velocities" that are responsible for the instability due to violation of the inf-sup condition. The algebraic terms able to govern the effects of the subscale velocities (SSV) are obtained by:

(i) imposing that the SSV satisfy a momentum-like equation to which is added a suitable function;

(ii) orthogonalizing the space for the approximation of the SSV to the space V_h in which the physical velocity $\boldsymbol{u_h}$ has to be approximated.

This technique allows us in particular to deal with convection dominated flows and to use equal-order velocity pressure interpolations. We apply this technique to complete the formulation (36 – 41).

Final algebraic stabilized system including the energy equation

Thus, in order to stabilize (36 – 41), we have added the suitable algebraic terms to equations of the momentums and the Poisson equation of the pressure, to get:

$$\begin{aligned}(\mathbf{M} + \nu\Delta t\mathbf{A})\tilde{\boldsymbol{u}}^{n+\frac{1}{2}} &= \Delta t\{-\mathbf{B}^T\boldsymbol{p}^n + \mathbf{M}\boldsymbol{f}_u^{n+1} - \tau(\mathbf{A} - \mathbf{B}^T\mathbf{M}_L^{-1}\mathbf{B}^T)\boldsymbol{p}^n\} \\ &\quad + \mathbf{M}\boldsymbol{u}^n(\tilde{\boldsymbol{x}}_{ft})\end{aligned} \tag{58}$$

$$\begin{aligned}(\mathbf{M} + \nu\Delta t\mathbf{A})\tilde{\boldsymbol{v}}^{n+\frac{1}{2}} &= \Delta t\{-\mathbf{C}^T\boldsymbol{p}^n + \mathbf{M}\boldsymbol{f}_v^{n+1} - \tau(\mathbf{A} - \mathbf{C}^T\mathbf{M}_L^{-1}\mathbf{C}^T)\boldsymbol{p}^n\} \\ &\quad + \mathbf{M}\boldsymbol{v}^n(\tilde{\boldsymbol{x}}_{ft})\end{aligned} \tag{59}$$

$$\begin{aligned}[(\Delta t + \tau)\mathbf{A} - \tau(\mathbf{B}^T\mathbf{M}_L^{-1}\mathbf{B}^T + \mathbf{C}^T\mathbf{M}_L^{-1}\mathbf{C}^T)]\boldsymbol{p}^{n+1} \\ = \Delta t\mathbf{A}\boldsymbol{p}^n - \left[\mathbf{B}^T\tilde{\boldsymbol{u}}^{n+\frac{1}{2}} + \mathbf{C}^T\tilde{\boldsymbol{v}}^{n+\frac{1}{2}}\right]\end{aligned} \tag{60}$$

where τ is a weight parameter and $\mathbf{M_L}$ is the lumped mass matrix. We also have the equations for the correction of the velocity fields, given by:

$$\mathbf{M}\boldsymbol{u}^{n+1} = \mathbf{M}\tilde{\boldsymbol{u}}^{n+\frac{1}{2}} - \Delta t\mathbf{B}^T\tilde{\boldsymbol{p}}^{n+1} \tag{61}$$

$$\mathbf{M}\boldsymbol{v}^{n+1} = \mathbf{M}\tilde{\boldsymbol{v}}^{n+\frac{1}{2}} - \Delta t\mathbf{C}^T\tilde{\boldsymbol{p}}^{n+1} \tag{62}$$

With the energy equation written in terms of the temperature and its corresponding boundary conditions (5)–(7) to the final algebraic stabilized formulation (58)–(62) of the problem (1)–(7), we can add the equation:

$$(\mathbf{M} + \Gamma\Delta t\mathbf{A})\mathbf{T}^{n+1} = \Delta t\mathbf{M}\mathbf{S}^{n+1} + \mathbf{M}\mathbf{T}^n(\tilde{\boldsymbol{x}}_{ft}) \tag{63}$$

Remark 5. We recall that in our stabilization process we do not have to include the convective terms.

4.3. Choice of the weight parameter τ

According to Codina and Soto (2004), a scheme is suggested that expresses τ in terms of the kinematic viscosity ν, the modulus of the velocity $\boldsymbol{u}^*$ (which is the sum of the computed velocity $\boldsymbol{u}_h$ and of the subscale velocity) and a characteristic length h. The formula of the weight τ is:

$$\tau = \left(c_1 \frac{\nu}{h^2} + c_2 \frac{|\boldsymbol{u}^*|}{h} \right)^{-1} \tag{64}$$

where c_1 and c_2 are suitable constants; it can be simplified as:

$$\tau = c_3 \frac{h^2}{\nu + |\boldsymbol{u}^*| h} \tag{65}$$

The characteristic length h can be estimated as the ratio between the modulus of two vectors $\boldsymbol{h}$ and $\boldsymbol{k}$, and represents the modulus of the Jacobian of the transformation of the generic element of the partition into the reference element, multiplied for a suitable constant c_4 (for triangular elements $c_4 = 0.7$). In order to simplify the procedure we choose for vector $\boldsymbol{k}$ the hypotenuse of the reference triangle, and for vector $\boldsymbol{h}$ the corresponding edge of the generic element. In this case $c_4 = 0.5$. Another simplification of the estimation of $\boldsymbol{h}$ could be by choosing the smallest edge of the elements of the partition and multiplying its length by 0.5. In the section relevant to the numerical tests a sensitivity analysis of τ is carried out.

4.4. Numerical procedure

In summary, the fractional step works following these steps:

i) the velocity, pressure and temperature fields are given at time $t = t^n$;
ii) compute the intermediate velocity field from Equations (58) and (59);
iii) compute the pressure field at time $t = t^{n+1}$ from Equation (60);
iv) correct the intermediate velocity field from Equations (61) and (62);
v) compute the temperature field at time $t = t^{n+1}$ from Equation (63);
vi) go to step (i) and repeat the above procedure until the desired solution is obtained.

5. Test cases

5.1. Two dimensional time-dependent problem

We have used an analytical solution of the Navier–Stokes equations similar to that of Zang, Street, and Koseff (1994) as benchmark to our approach (and also to check the performance of our in-house code). The following is the solution to the two dimensional unsteady flow of decaying vortices:

$$u = -\cos(\pi x)\sin(\pi y) exp(-2t) \tag{66}$$

$$v = \sin(\pi x)\cos(\pi y)\exp(-2t) \tag{67}$$

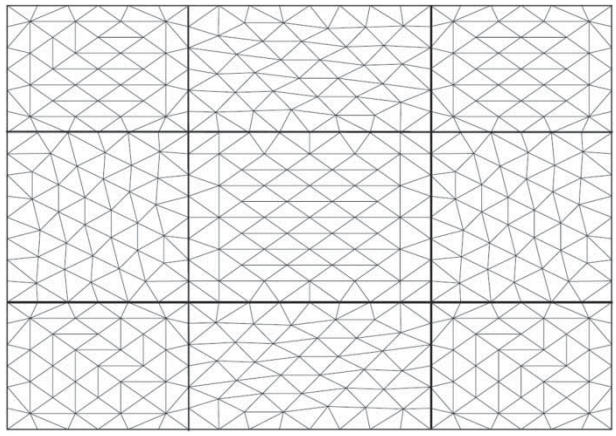

Figure 2. Problem 5.1: mesh with 1569 nodes and nine subdomains for the Schwarz preconditioner.

Table 1. Problem 5.1, L^∞-error norm for $\tau = 1.000\text{E}-5$, $\Delta t = 5.000\text{E}-3$, $N_{TS} = 200$, $u_{max} = 1.353\text{E}-1$, $v_{max} = 1.353\text{E}-1$, $p_{max} = 9.157\text{E}-3$ and various Re.

Re	1.000 E+2	4.000 E+2	1.000 E+3	5.000 E+3
e_u	9.407 E-4	2.374 E-3	3.811 E-3	7.217 E-3
e_v	7.098 E-4	1.538 E-3	3.845 E-3	6.354 E-3
e_p	7.964 E-3	6.452 E-3	5.403 E-3	4.921 E-3

$$p = -\frac{1}{4}[\cos(2\pi x) + \cos(2\pi y)]\exp(-4t) \tag{68}$$

$$f_u = 2(1 - \nu\pi^2)\cos(\pi x)\sin(\pi y)\exp(-2t) \tag{69}$$

$$f_v = 2(-1 + \nu\pi^2)\sin(\pi x)\cos(\pi y)\exp(-2t) \tag{70}$$

where f_u and f_v are the source terms. The initial and boundary conditions are obtained from the analytical solution. Instead of $\Omega = [0, \pi]^2$, we have chosen the domain $\Omega = [0, 1]^2$ and the computational mesh used has 1569 nodes, as represented in the Figure 2. We have taken the viscosity $\nu = \frac{1}{Re}$ where Re is the Reynolds number and various Reynolds numbers have been used ($Re = 100$, 400, 1000 and 5000). The length of the smallest edge is $l = 4.600\text{E}-2$ so that the estimation of characteristic length h, based on the second rule, is $h = 2.300\text{E}-2$; the time increment used is $\Delta t = 5.000\text{E}-3$and we used 200 time steps to reach the final time $t = 1$. This problem has also been used by previous researchers such as Feraudi and Pennati (1997), Kim and Moin (1985), Patankar (1980), to test the accuracy of their numerical methods. By denoting e_u, e_v and e_p the L^∞–error norms of the two components of the velocity and of the pressure respectively, u_{max}, v_{max} and p_{max} the maximum of the analytical velocity and pressure, N_{TS} the total number of time increments, we present in Table 1 the accuracy obtained at the final time $t = 1$. Figure 3 shows the streamlines and Figure 4 depicts the directions of the flow inside the domain, while Figure 5 illustrates the pressure contours (both for analytical and numerical solutions at time $t = 1$ for $Re = 5000$). Table 2 shows the performance of the Schwarz preconditioner for

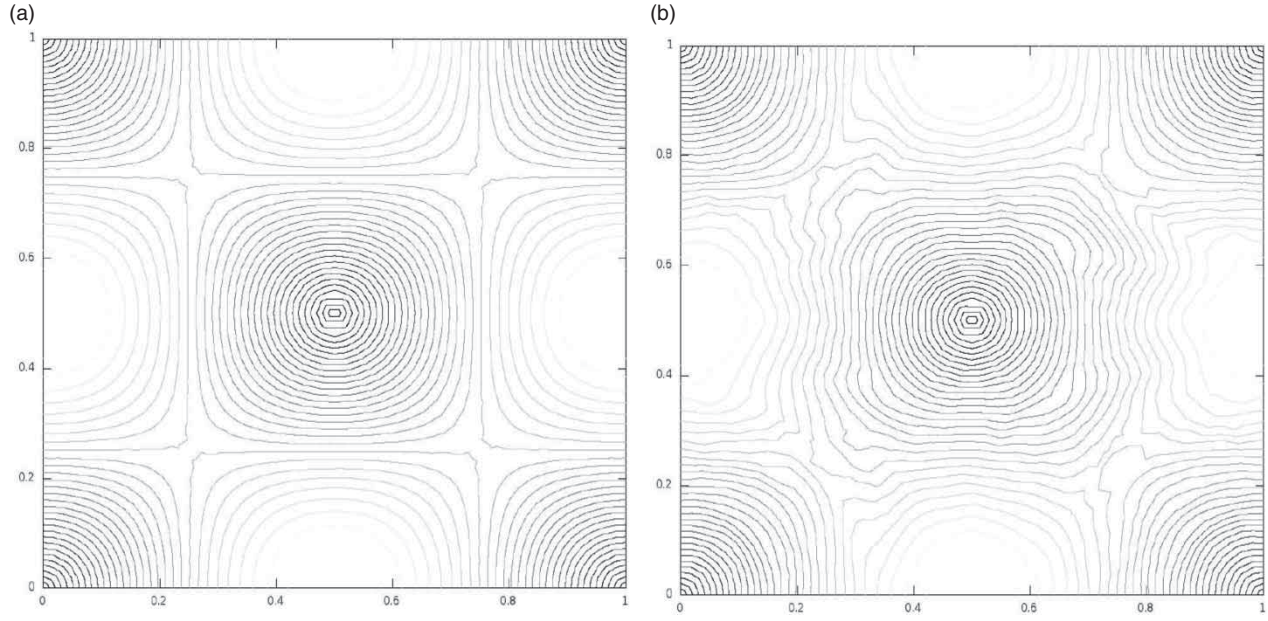

Figure 3. Problem 5.1 $Re = 5000$: streamlines of the analytical (a) and numerical (b) solutions.

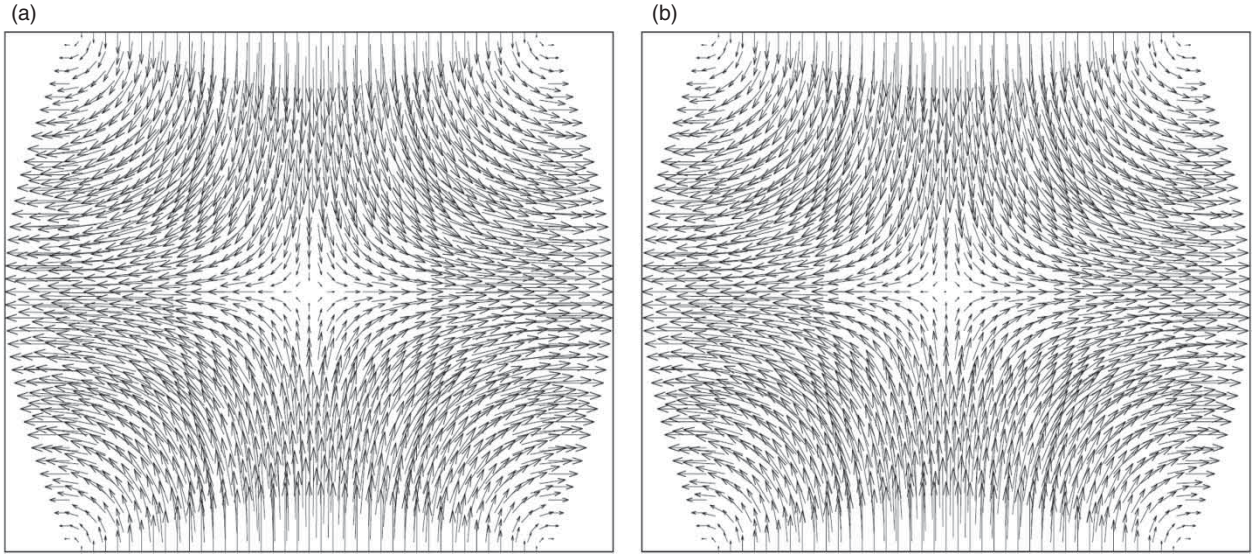

Figure 4. Problem 5.1 $Re = 5000$: velocity vectors of the analytical (a) and numerical (b) solutions.

the case resolved. In all the four tests, in order to simplify the calculations, we chose $\tau = 1.000\text{E}-5$. This value was not calculated by the formula in (65), but by choosing in an heuristic way a suitable value for c_3. Nevertheless we should keep in mind that in the formula (64) there are the two constants c_1 and c_2 and that the good results obtained for all the numerical tests with the same value of τ, show the great flexibility in the choice of τ. In the next problem a broader analysis about the influence of τ on the results will be given.

Remark 6. In all the tests solved (both in this problem as in the others problems) the Schwarz preconditioner was used with, substantially, the same reduction of the iteration number.

5.2. Lid-driven cavity problem with analytical solution

This problem has been used by Shih and Tan (1989) and it represents the isothermal recirculation flow in a square cavity generated by the uniform translation of the upper surface (lid) of a cavity whose exact solution is given by:

$$u = 8f(x)g'(y) = 8(x^4 - 2x^3 + x^2)(4y^3 - 2y) \tag{71}$$

$$v = -8f'(x)g(y) - 8(4x^3 - 6x^2 + 2x)(y^4 - y^2) \tag{72}$$

$$p = \frac{8}{Re}[F(x)g''(y) + f'(x)g'(y)] + 64F_1(x)\{g(y)g''(y) - [g'(y)]^2\} \tag{73}$$

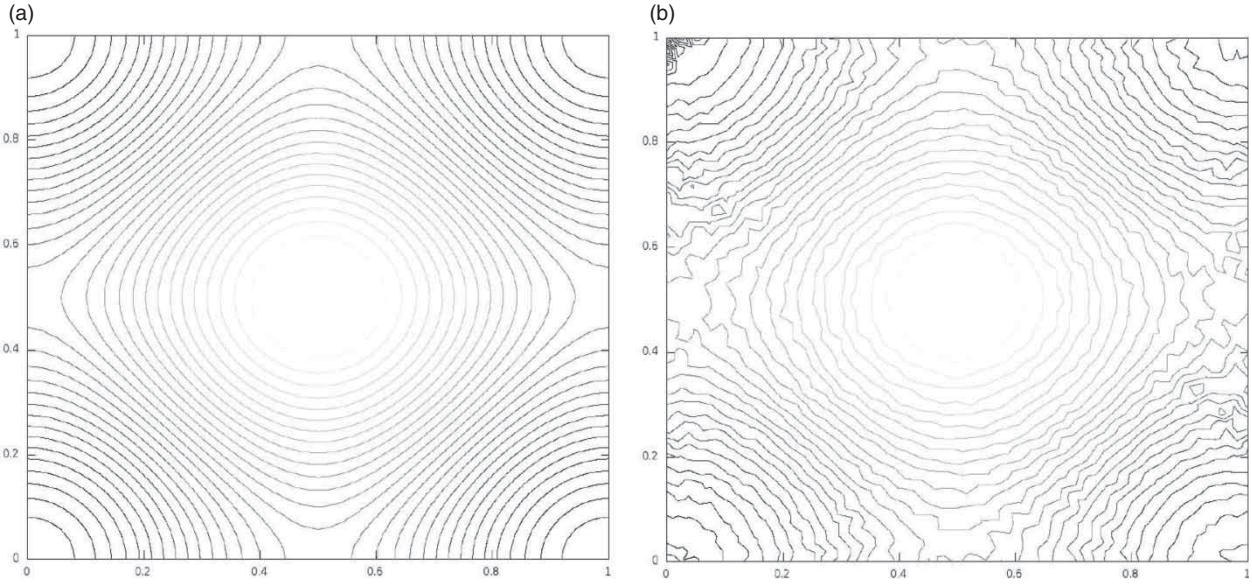

Figure 5. Problem 5.1 $Re = 5000$: pressure contours of the analytical (a) and numerical (b) solutions.

Table 2. Problem 5.1, Condition numbers K ($\mathbf{A}_h$) and K ($\mathbf{P}_{asc}^{-1}\mathbf{A}_h$) of the not preconditioned and of the preconditioned matrices, and iteration numbers ≠ Iters and ≠ Iters_p for the solution of the non-preconditioned and preconditioned systems for various values of *Re*.

Re	$\mathbf{A}_h$ of variables	K ($\mathbf{A}_h$)	K ($\mathbf{P}_{asc}^{-1}\mathbf{A}_h$)	≠ Iters	≠ Iters _p
100	$\tilde{u}^{n+\frac{1}{2}}, \tilde{v}^{n+\frac{1}{2}}$	5.945E + 0	3.576E + 0	13	4
	p^{n+1}	5.687E + 8	4.011 E + 4	256	22
	u^{n+1}, v^{n+1}	6.238E + 0	3.623E + 0	16	5
400	$\tilde{u}^{n+\frac{1}{2}}, \tilde{v}^{n+\frac{1}{2}}$	5.667E + 0	3.599E + 0	16	5
	p^{n+1}	5.687E + 8	4.011E + 4	259	22
	u^{n+1}, v^{n+1}	6.238E + 0	3.623E + 0	16	5
1000	$\tilde{u}^{n+\frac{1}{2}}, \tilde{v}^{n+\frac{1}{2}}$	5.923E + 0	3.603E + 0	13	5
	p^{n+1}	5.687E + 8	4.011E + 4	258	22
	u^{n+1}, v^{n+1}	6.238E + 0	3.623E + 0	16	5
5000	$\tilde{u}^{n+\frac{1}{2}}, \tilde{v}^{n+\frac{1}{2}}$	6.150E + 0	3.606E + 0	13	5
	p^{n+1}	5.687E + 8	4.011E + 4	259	22
	u^{n+1}, v^{n+1}	6.238E + 0	3.623E + 0	16	5

where the source term with respect to u is:

$$f_u = 64 f(x) f'(x) [(g'(y))^2 - g(y)g''(y)] - \frac{8}{Re}(f''(x)g'(y) + f(x)g^{(3)}(y)) - \frac{8}{Re}[F'(x)g^{(3)}(y) + f''(x)g'(y)] - 64F_1'(x) \{g(y)g''(y) - [g'(y)]^2\} \quad (74)$$

the source term with respect to v is:

$$f_v = 64g(y)g'(y)[-f(x)f''(x) + (f'(x))^2] + \frac{8}{Re}(f^{(3)}(x)g(y) + f'(x)g''(y)) - \frac{8}{Re}[F(x)g^{(4)}(y) + f'(x)g''(y)] - 64F_1(x)\{g'(y)g''(y) + g(y)g^{(3)}(y) - 2g'(y)g''(y)\} \quad (75)$$

Where: $f(x) = x^4 - 2x^3 + x^2, \quad g(y) = y^4 - y^2,$

$$F(x) = 0.2x^5 - 0.5x^4 + \frac{x^3}{3},$$

$$F_1(x) = 0.5[f(x)]^2$$

and the primes of *f(x)* and *g(y)* denote the differentiation with respect to *x* and *y,* respectively. In Figure 6 we present the domain and the boundary conditions for the velocity, at the pressure we assign homogeneous Neumann conditions. We have chosen the domain $\Omega = [0,1]^2$ and the viscosity $\nu = 0.01$.We solved the stationary problem by an iterative process starting with the rest condition, advancing along a fictitious transient and ending with a suitable stopping criteria (in other words, was built an iterative cycle with relaxing parameter $\Delta t = 0.05$, and at every iteration a fractional step scheme was applied so that the resulting algebraic systems were solved by the preconditioned

Table 3. Problem 5.2 $Re = 100$: L^{∞}-error norm for various τ. $u_{max} = 1.000E+0$, $v_{max} = 3.838E-1$ and $p_{max} = 6.399E-2$.

τ	2.000 E-3	2.000 E-4	2.000 E-5	2.000 E-6
e_u	2.823 E-2	2.491 E-2	2.605 E-2	2.614 E-2
e_v	2.330 E-2	1.753 E-2	1.834 E-2	1.839 E-2
e_p	2.615 E-1	2.119 E-1	2.849 E-2	2.808 E-2

iterative method Bi-CGSTAB). We have chosen to stop the iterative process when the differences of the maximum values of the velocities and pressure at time instant n and $n + 1$ are less than a fixed value ϵ (e.g., $\epsilon = 10E-6$). We have computed the L^{∞} −error norms of the numerical solutions generated by the new method and have reported them in the Table 3. We would point out that as the analytical solution is known, a strict control of the numerical results is possible. Figure 2 shows the mesh of 1569 nodes used, and Figures 7 and 8 present the streamlines and the vectors of the analytical and numerical velocities respectively. In Figure 9 the contours of pressure are shown. The value calculated by the simple rule (65) for $c_3 = 1.$ is $\tau = 1.500E-2$. It is interesting to note that the analytical velocity field is not directly influenced by the Reynolds parameter, but the Reynolds value changes the expressions of the pressure and the source term. Keeping this in mind, the graphics of Figures 7, 8 and 9 seem regular and coherent. From Table 3 we can deduce that the variation of τ affects (like expected) the accuracy but not the stability (at least for a quite large range of its values) of the results and that the errors of the velocity components are quite low.

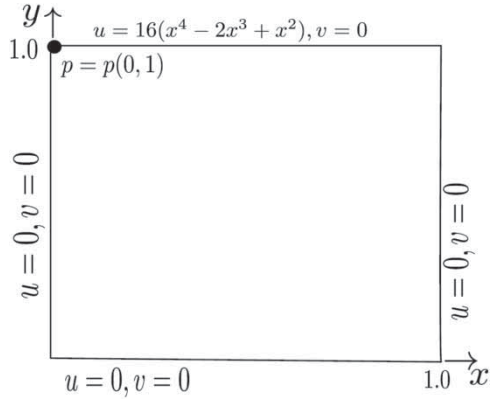

Figure 6. Problem 5.2: boundary conditions.

5.3. *Lid-driven problem with constant boundary conditions*

This problem has been used by Bruneau and Saad (2006) and it is similar to problem 5.2 except for the boundary condition of $\boldsymbol{u}$ on the top boundary where it takes the constant value 1. The analytical solution of this problem is unknown, however, it is a classical test for checking the efficiency of new algorithms. In fact, the lid-driven cavity problem is considered the prototypical recirculation flow because the streamlines pattern exhibits a central primary vortex and for high Reynolds number ($Re \geq 1000$) the possible formation of counter-rotating secondary vortices at the bottom corners of the cavity. In order to check the accuracy and the computational efficiency of the proposed method, we compare our results of problem 5.3 (with $Re = 1000$) with those found in four recent papers (Han et al., 2013; Kumar et al., 2010; Kumar et al., 2009; Pai et al.,

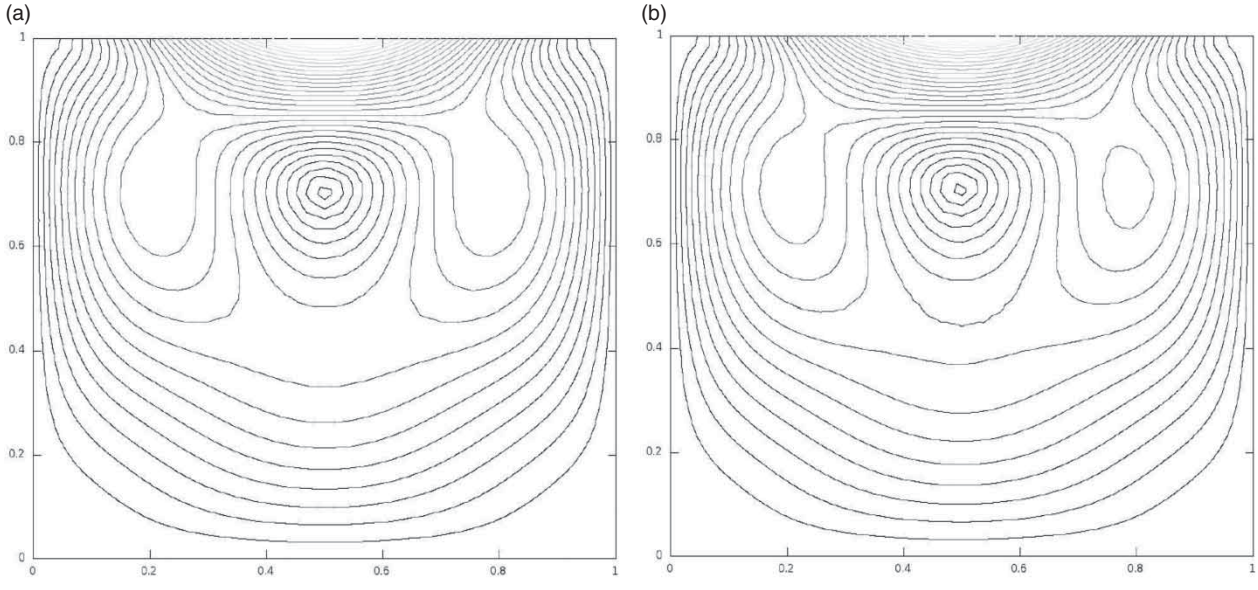

Figure 7. Problem 5.2 $\tau = 2E-5$: streamlines of the analytical (a) and numerical (b)solutions.

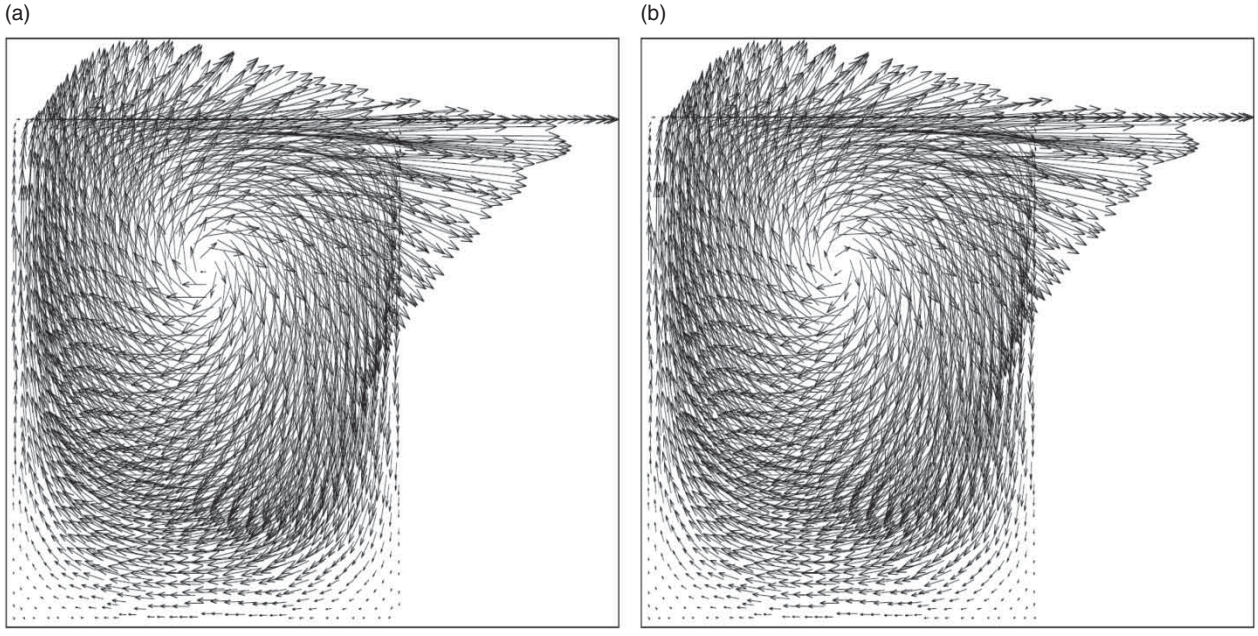

Figure 8. Problem 5.2 $\tau = 2E\text{-}5$: velocity vectors of the analytical (a) and numerical (b)solutions.

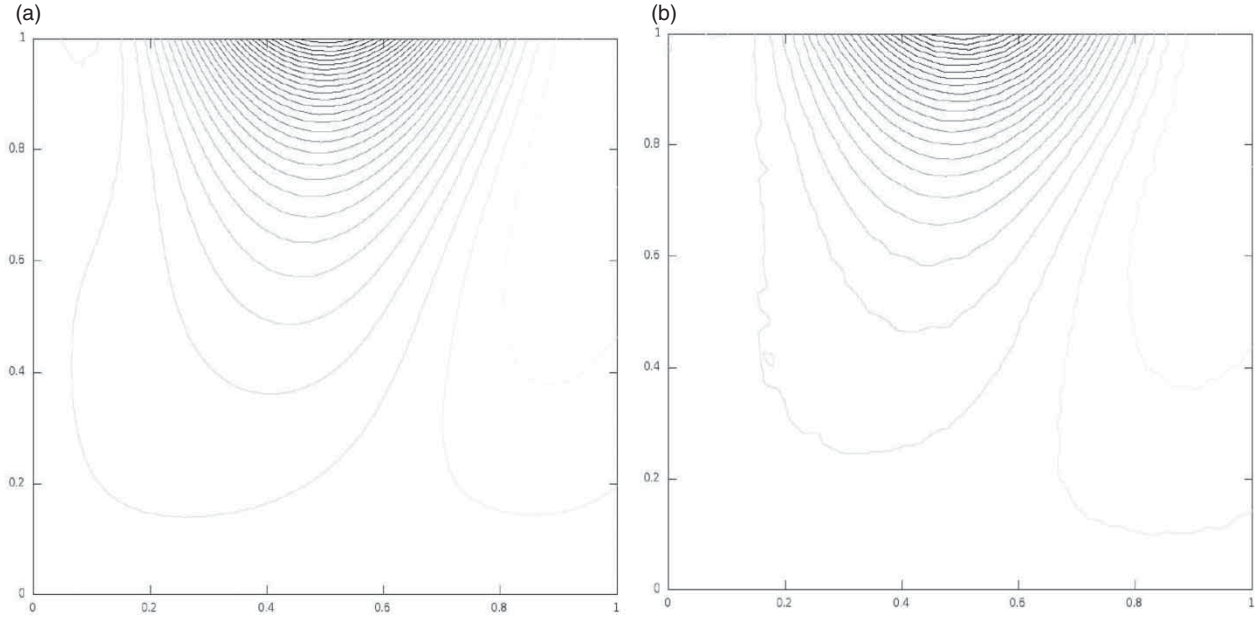

Figure 9. Problem 5.2 $\tau = 2E\text{-}5$: pressure contours of the analytical (a) and numerical (b)solutions.

2013). In these papers the problem 5.3 (and other problems) was solved by using different numerical techniques, with different meshes or grids. A short presentation of the tests developed in the papers is as follows. In the first paper (Kumar et al., 2009) the spatial discretization was realized with colocated grids and by cell-centred FV where the convective flux was approximated by the QUICK scheme and the diffusion flux by the central second-order FD formula. To solve the coupled system, a SIMPLEC algorithm was applied and in order to reduce the computing time and obtain a grid independent convergence rates, a multigrid method with full approximation scheme and four grid levels was adopted. In order to see the secondary vortices a uniform grid of 513×513 volumes (263,000 grid points) was necessary, because the solution obtained by a grid of 129×129 volumes (16,641 grid points) did not show the secondary vortices. The computational effort of the multigrid *V-cycle* was of 32 work units, and the number of iterations (for the grid of 129×129 volumes) required to reach the grid convergence with a fixed tolerance $\epsilon = 10E-8$, was 1500 (without multigrid 14,500 iterations were necessary to reach the convergence). In the second paper (Kumar et al., 2010) the target to save computing time while maintaining a high accuracy, was sought

by using nonuniform staggered grids in the physical space and clustering the grid points in the regions of large gradients. Since the spatial approximation was carried out by FD formulas, a transformation into a computational space with uniform grids was made. Unfortunately the transformed equations show a greater number of terms than the primitive equations. The time-advancing was obtained via a second-order non incremental fractional-step method. To improve the computational efficiency, the pressure Poisson equation (that is the most expensive computational kernel) was solved at every time step by a multi grid technique. The *V-cycle* of four level grids, with a computational effort of 36 work units, produced a good time-wise gain for the lid-driven problem at $Re = 3200$, discretized with a 129×129 grid. In the study of the lid-driven problem at $Re = 1000$, the 129×129 grid and $\Delta t = 0.001$ were used. In some figures the time evolutions of the streamline patterns, until the steady state, are shown. Through them we can deduce that at time $t = 5$ two recirculation zones start to be present, at $t = 10$ two secondary vortices arise at the bottom corners, at $t = 40$ the two secondary vortices are almost completely shaped. In the third paper (Han et al., 2013), the authors solved the 2D Navier–Stokes equations in primitive variables by means of a FE approach in which the elements are nine-node quadrilaterals both for velocities and pressure. The convective term was approximated by a semi-implicit form of three steps Taylor-characteristic-based-split scheme, while the diffusive term by the usual FE technique (namely by the stiffness matrix). The time-advancing is declared to be an incremental fractional-step method (even if from the equations (26) and (27) it can be deduced that is of non-incremental kind). The domain of the lid-driven test was partitioned with 20×20 elements in a structured adaptive way; for the marching temporal discretization $\Delta t = 0.005$ was chosen and the computations were stopped when the L^2-norm error was lower than $10E-5$. For the case $Re = 1000$, the streamlines velocity figure is not given, while the vertical and horizontal profiles of the velocities at the cavity center at the final state of the transient are shown. No information about the solution of the algebraic systems is reported. In the fourth paper (Pai et al., 2013), the lid-driven cavity problem was used like a precursor model for studying mixer designs. The 2D Navier–Stokes equations were solved by the commercial code FLUENT which employs FV for the discretization in space and the SIMPLE algorithm for time-advancing. The nonuniform grid used was finest near the no-slip wall boundary and it had 100 grid-points along walls for a total number of 17,730 volumes. The value of Δt, considered good enough to capture the physics of the problem, was $\Delta t = 0.001$. We solved, by the same approach as followed in the previous problem, the case with $\mathrm{Re} = 1000$. The mesh used is represented in Figure 10, it was created by the TRIANGLE package (Joe, 1991) respecting an adaptive criteria, that is, using elements with smaller diameter in the regions where higher gradients are expected. It has 3009 nodes, with $hmin = 2.1E-2$, $hmax = 7.9E-2$. The other parameters used were $\tau = 2.0E-5$, $\Delta t = 0.05$ and $\epsilon = 10E-8$. In Figure 11 are represented the velocity vectors at $t = 80$ and in it is possible to single out the central primary vortex and, at the bottom corners, the well-known secondary vortices. The zooms of the secondary vortices are represented in Figure 12. In Figure 13 are plotted the profiles of the u and v velocity components along the vertical and horizontal centerlines. The comparison of the graphics shown in Figures 12 and 13 and those in some of the above papers (Han et al., 2013; Kumar et al., 2010; Pai et al., 2013) point out some differences; in particular the velocity profiles appear to be affected by viscous effects. All that should not be surprising because the graphics are built by the interpolation of the nodal values calculated by means of a quite coarse mesh (it has only 3009 nodes). In the numerical simulations the maximum values of Courant number was $C = 2.5$ and of Peclet number was $P_e = 79$. The computational efficiency is confirmed by the particularly low number of iterations of the Schwarz preconditioned Bi-CGSTAB iterative solver used to solve the momentum equations, the pressure equation and the velocity and pressure correction equations (5 and 5, 21, 5 and 5 iterations, respectively). The CPU time corresponding to each of the above iterations was 0.024s for the momentum equation, 1.005s for the pressure equation and 0.020s for the velocity and pressure correction equations, on a Sony VAIO Series EA46FMW personal computer.

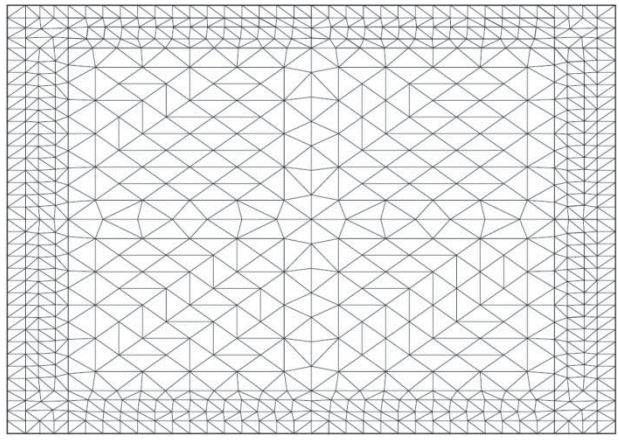

Figure 10. Problem 5.3: mesh with 3009 nodes.

Some comments regarding our results are appropriate. The use of an adaptive mesh (not requiring any transformation) and the numerical schemes used in our approach make possible to capture the physics of the problem (in particular the presence of secondary vortices at $Re = 1000$) also with a small number of nodes. The approximation of the convective terms by characteristics allows to obtain good results even in presence of very high Peclet and Courant numbers; moreover, the solution of the algebraic systems calculated by means of preconditioned iterative

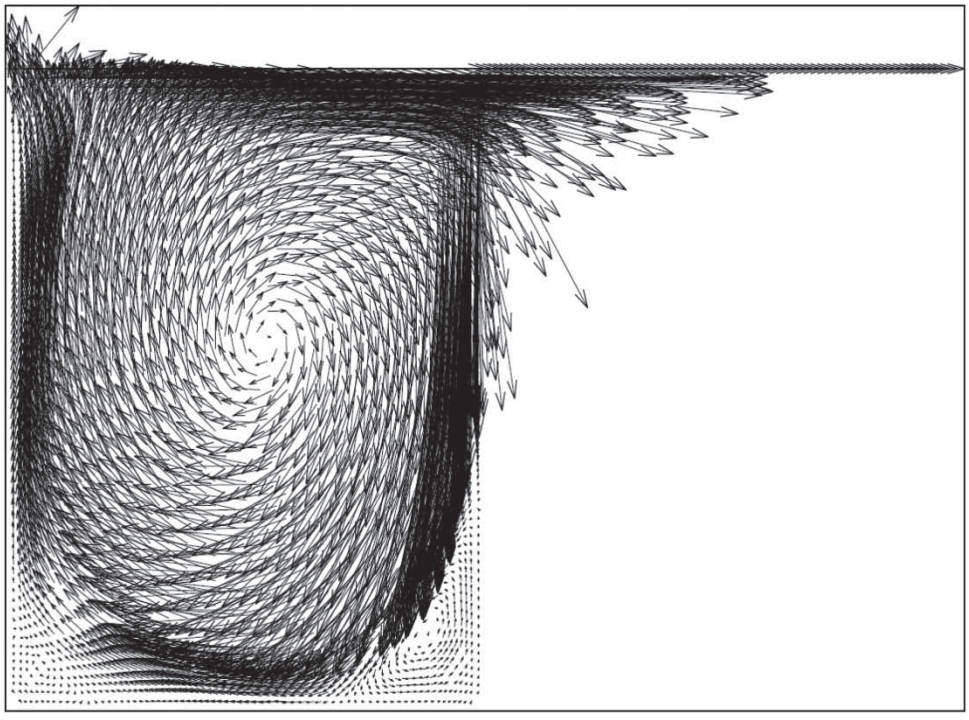

Figure 11. Problem 5.3: velocity vectors at $t = 80$.

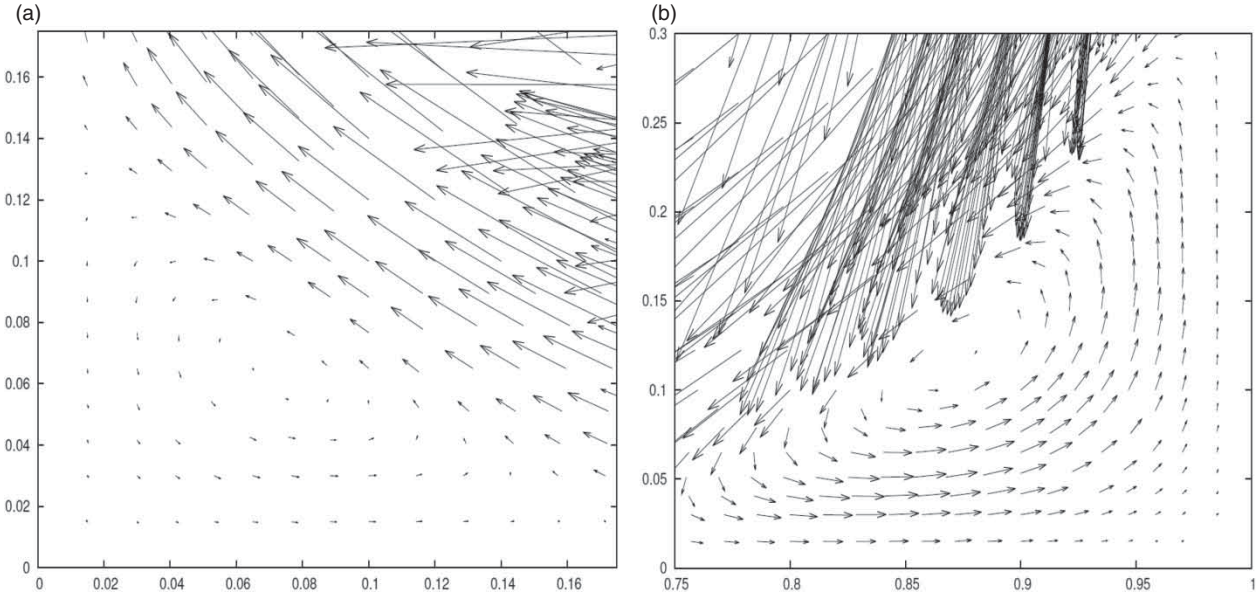

Figure 12. Problem 5.3: zoom of the secondary vortices, left (a) and right (b) corner.

solvers allows to compare the computational efficiency of our approach with that of the multigrid solvers.

5.4. *Thermal convection in a square cavity*

In this section, we consider a benchmark flow problem where no analytic solution is known, but considered very important by the researchers. The aim is to compare our results to some of well-established schemes present in the literature for a natural convection in a square cavity problem. In particular in De Vahl Davis (1983) is reported the definition and the results of a large number of tests along with some significant reference values. In the problem, is examined the flow of a fluid inside a square cavity for which the top and the bottom walls are kept to be adiabatic and the vertical walls are kept to be isothermal at temperatures $T_c = -0.5$ and $T_h = 0.5$ respectively (see Figure 15). Initially the fluid is assumed

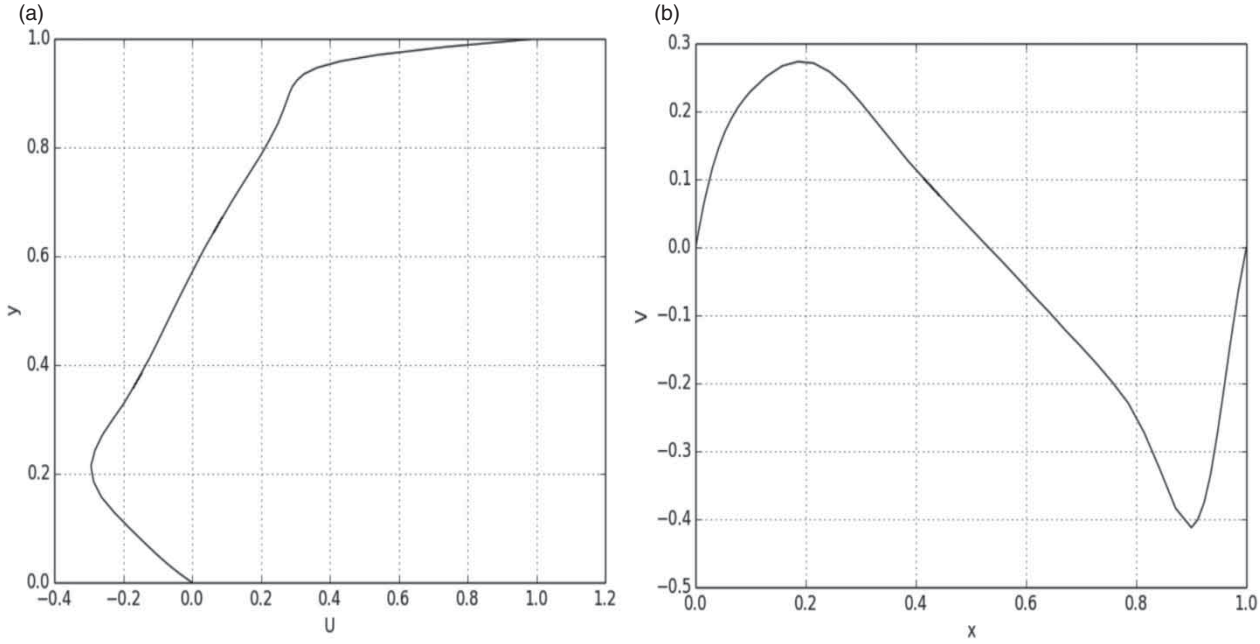

Figure 13. Problem 5.3: profiles of u and v velocity components along the vertical (a)and horizontal (b) centerlines.

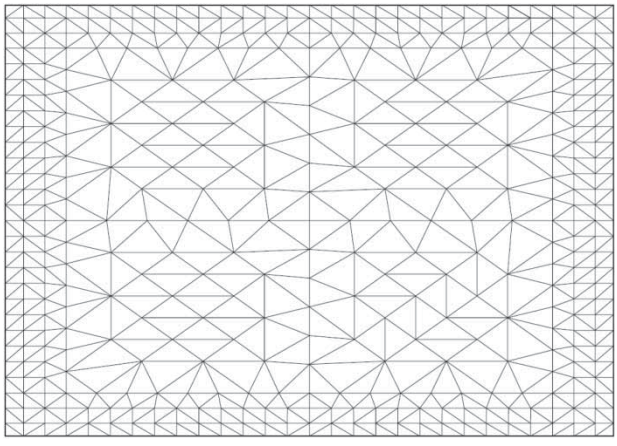

Figure 14. Problem 5.4: mesh with 1761 nodes.

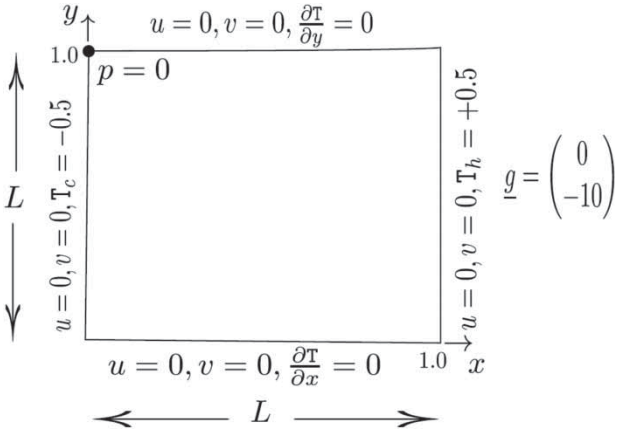

Figure 15. Problem 5.4: boundary conditions.

to be at rest at temperature $T = 0$; then the temperature at the vertical walls begins to change and the fluid is subjected to a phenomenon of convection due to the thermal gradient. We assumed that the fluid is incompressible such that the Boussinesq approximation holds, that is $\boldsymbol{f} = \rho \boldsymbol{g} \alpha (T - T_r)$. By this benchmark problem, we want to check the behavior of the solution taking into account the estimation of τ in different situations both with respect to the physical and the computational situations. Therefore, for the mesh of Figure 14 with 1761 nodes, the length of the smallest edge is $l = 3.600\text{E}-2$ so that $h = 1.800\text{E}-2$, for the mesh of Figure 10 with 3009 nodes, the length of the smallest edge is $l = 2.1\text{E}-2$ so $h = 1.05\text{E}-2$. The results obtained after 200 steps with $\Delta t = 5.000\text{E}-3$ for various values of Rayleigh (Ra), Reynolds (Re) and Prandtl (Pr) numbers on the meshes of Figures 10 and 14 are reported in Tables 4 and 5. In Figures 16 and 17 are plotted the velocity vectors and the temperature contours for the case with $Ra = 3.5\text{E} + 5$. Through them it can be seen that both the distributions are very close to those expected. The results presented in Table 4 show that the solutions of problem 5.4 are strongly dependent on the physical parameters (besides, obviously, the mesh rates), for example one can see that for $Ra = 10\text{E}+4$ and $Pr = 7.1\text{E}-1$ the velocity components double their values with respect to the case with $Pr = 7.1\text{E}-2$. Moreover, it can be seen that the dependence from the physical parameters becomes more and more important for increasing Ra values, a clear example of this fact is the variation of the velocity values for the cases $Ra = 10\text{E}+5$, $Pr = 7.1\text{E}-1$ that give $Re = 1.260\text{E}+2$, and $Ra = 3.510\text{E}+5$, $Pr = 4.0\text{E}-2$ that give $Re = 1.755\text{E}+3$.

Table 4. Problem 5.4: u_{max} and v_{max} for various Ra, Re, Pr, τ_c is the computed value of τ from formula (65) with $c_3 = 1.$ and τ_u the used value of τ.

	Mesh 10			Mesh 14		
τ_u	1.100 E-4	1.100 E-4	2.500 E-4	1.000 E-5	3.500 E-5	3.300 E-5
τ_c	2.400 E-4	9.900 E-5	2.500 E-4	2.700 E-4	3.300 E-4	3.200 E-4
Pr	5.000 E-2	7.100 E-1	4.000 E-2	7.100 E-1	7.100 E-2	5.000 E-2
v	5.000 E-2	7.100 E-1	4.000 E-2	7.100 E-1	7.100 E-2	5.000 E-2
u_{max}	3.234 E + 1	4.897 E + 1	3.738 E + 2	1.624 E + 1	3.004 E + 1	3.112 E + 1
v_{max}	4.344 E + 1	7.591 E + 1	5.936 E + 2	1.923 E + 1	4.067 E + 1	4.294 E + 1
Re	1.083 E + 3	1.270 E + 2	1.755 E + 3	3.500 E + 1	7.120 E + 2	1.060 E + 3
Ra	10 E + 4	10 E + 5	3.5 E + 5	10 E + 4	10 E + 4	10 E + 4

Table 5. Problem 5.4: comparison with available benchmark solutions.

Solutions	Results	$Ra = 10\text{E} + 4$	$Ra = 10\text{E} + 5$	$Ra = 3.5\text{E} + 5$
Proposed	u_{max}	1.624E + 1	4.897E + 1	3.738E + 2
	v_{max}	1.923E + 1	7.591E + 1	5.936E + 2
	Re	3.500E + 1	1.270E + 2	1.755E + 3
	Pr	7.100 E-1	7.100 E-1	4.000 E-2
(De Valh Davis, 1983)	u_{max}	1.617E + 1	3.473E + 1	
	v_{max}	1.961E + 1	6.859E + 1	
	Re	3.500E + 1	1.082E + 3	
(Hookey & Baliga, 1998)	u_{max}	1.620E + 1	3.493E + 1	
	v_{max}	1.947E + 1	6.912E + 1	
	Re	3.500E + 1	1.090E + 3	
(Malan et al., 2002)	u_{max}	1.617E + 1	3.495E + 1	
	v_{max}	1.980E + 1	6.866E + 1	
	Re	3.600E + 1	1.085E + 3	

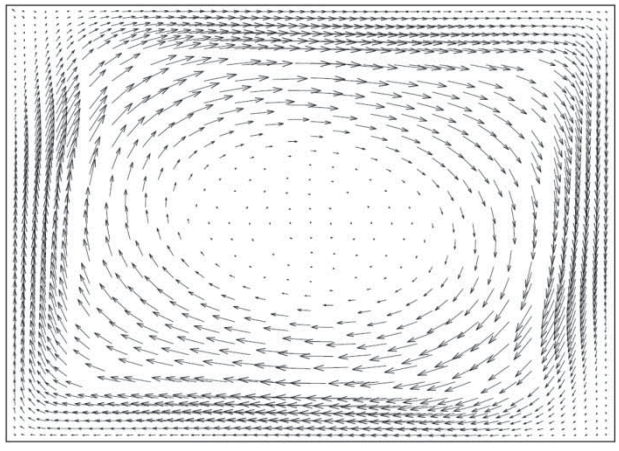

Figure 16. Problem 5.4 $Ra = 3.5\text{E} + 5$ and $Re = 1755$: velocity vectors at $t = 1$.

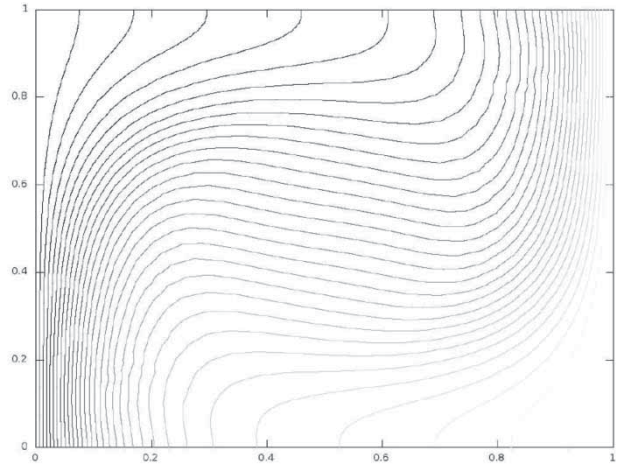

Figure 17. Problem 5.4 $Ra = 3.5\text{E} + 5$ and $Re = 1755$: temperature contours.

6. Concluding remarks

In this paper, a cost-effective approach for the solution of 2D incompressible Navier–Stokes equations has been addressed. The new method obtains an optimal compromise between numerical properties (stability and accuracy) and computational efficiency (simplicity and flexibility). The most important features of the new model are: using polynomials of degree two (both for velocities and pressure) in an FE spatial approximation; time-advancing by a fractional step approach in which the nonlinear convective term is approximated by characteristics; adding a suitable stabilization technique in order to overcome the instabilities inherent in the equal-order choice. In this way the computational kernels are reduced to elliptic-like ones for

whose solution very efficient solution techniques are available. In fact the algebraic systems are solved by iterative solvers preconditioned with Schwarz additive scalable preconditioners. The new model has been tested, by solving several well-known problems, some with analytical solution. This allowed us to check both the accuracy of the results and the effectiveness of the simple rule used for the estimation of the weight τ involved in the stabilization technique. The several numerical experiments carried out prompt one to conclude that the rule is robust, in fact in our test the value of τ was constant during the transient and in every point of the domain, even when anisotropic meshes were used. The formal comparison (i.e., number of iterations used in the solution of the algebraic systems of the test problem 5.3) among the numerical techniques adopted in the presented model and the ones adopted in other similar models, allow us to conclude that the objective of the work has been reached.

Some improvements and generalizations could be developed; for example the spatial approximation based on polynomials of degree two could be substituted with polynomials of degree three, obtaining a better accuracy both for the convective and diffusive terms, or the temporal approximation could be improved by a Crank-Nicolson scheme. Both these choices should not excessively increase the computational time. Moreover, being the computational kernels of elliptic kind, the feasibility to apply well-established *h-adaptive* techniques could be advantageously adopted (Naga & Zhang, 2004).

Furthermore, the presented method could be suitably generalized to the solution of moving boundary CFD problems. In particular, the time approximation based on the marching scheme and the fractional step method, the spatial approximation based on the characteristics and (probably) on FE with serendipity third-degree polynomial basis, and the Schwarz preconditioned iterative solvers of the algebraic systems, make promising the extension of the presented method to 3D problems (e.g., 3D Navier–Stokes equations). The multidomain approach, formally used for the construction of the Schwarz preconditioner, could be considered like a starting point for developing distributed memory parallel computing algorithms, similarly to what made for the solution of 2D shallow water problems (Corti & Pennati, 1997).

A drawback of the presented method is the lack of local conservativity (drawback common to almost every FE approximation); this handicap could become particularly severe for 3D problems. In order to guarantee local conservation in the FE context, an approximation by cell-vertex FV is generally adopted, this choice requires the definition of a dual mesh leading to a high increase of the computational effort (particularly significant for 3D high-order FV). An option for the cell-vertex FV approximation could consist in the construction of conservative finite element methods; the development of such methods has already started (Kengni Jotsa, 2010; Kengni Jotsa, 2012; Kengni Jotsa & Pennati, 2013) and work is in progress along these directions.

Acknowledgements

Authors thank Prof. K.W. Chau and four anonymous reviewers for their valuable suggestions and comments improving the quality of the paper. Authors thank also Dr. J. Nashipu and Dr. B. Kometa for useful grammatical corrections of the manuscript.

References

Acharya, S., & Moukalled, F. H. (1989). Improvements to incompressible flow calculations on a non staggered curvilinear grid. *Numerical Heat Transfer*, *15*, 131–152.

Ali, J., Fieldhouse, J., & Talbot, C. (2011). Numerical modelling of three dimensional thermal surface discharges. *Engineering Applications of Computational Fluid Mechanics*, *5*(2), 201–209.

Baker, G. A., Dougalis, V. A., & Karakashian, O. A. (1982). On a higher order accurate fully discrete Galerkin approximation to Navier-Stokes equations. *Mathematics of Computation*, *39*, 339–375.

Bochev, P., Cai, Z., Manteuffel, T. A., & McCormick, S. F. (1998). Analysis of velocity-flux first order system least-squares principles for the Navier-Stokes equations. Part I. *SIAM Journal of Numerical Analysis*, *35*, 990–1009.

Brezzi, F., & Douglas, J. (1988). Stabilized mixed methods for the Stokes problem. *Numerische Mathematik*, *53*, 225–235.

Bruneau, C. H., & Saad, M. (2006). The 2D lid-driven cavity problem revisited. *Computers and Fluids*, *35*, 326–348.

Cavazzutti, M., Corticelli, M. A., Masina, G., & Saponelli, R. (2013). CFD analyses of syngas-fired industrial tiles kiln module. *Engineering Applications of Computational Fluid Mechanics*, *7*(4), 533–543.

Choi, H. G., Choi, H., & Yoo, J. Y. (1997). A fractional four-step finite element formulation of the unsteady incompressible Navier-Stokes equations using SUPG and linear equal-order finite element methods. *Computer Methods Applied Mechanics Engineering*, *143*, 333–348.

Codina, R. (2001). Pressure stability in fractional step finite element methods for incompressible flows. *Journal of Computational Physics*, *170*, 112–140.

Codina, R., & Badia, S. (2006). On some pressure segregation methods of fractional step type for the finite element approximation of incompressible flow problems. *Computer Methods Applied Mechanics Engineering*, *195*(23–24), 2900–2918.

Codina, R., & Soto, O. (2004). Approximation of the incompressible Navier-Stokes equations using orthogonal subscale stabilization and the pressure segregation on anisotropic finite element meshes. *Computer Methods Applied Mechanics Engineering*, *193*, 1403–1419.

Corti, S., & Pennati, V. (1997). Design environment simulations and implementation of the different parallelization strategies. Third deliverable of the PCECOWATER Project-PCI second initiative, Esprit Project 21039.

De Vahl Davis, G. (1983). A natural convection of air in a square cavity: A benchmark numerical solution. *International Journal for Numerical Methods in Fluids*, *3*, 249–264.

Deponti, A., Pennati, V., & De Biase, L. (2006). A fully 3D finite volume method for incompressible Navier-Stokes equations. *International Journal for Numerical Methods in Fluids*, *52*, 617–638.

Deponti, A., & Pennati, V., et al. (2006). A new fully 3D numerical model for ice dynamics. *Journal of Glaciology*, *52*(178), 365–376.

Donatelli, M., Molteni, M., Pennati, V., & Serra Capizzano S. (In press). Multigrid methods for cubic spline solution two points (and 2D) boundary value problems. *Applied Numerical Mathematics*. doi:10.1016/j.apnum.2014.04.004.

Douglas, J., & Wang, J. (1989). An absolutely stabilized finite element method for the Stokes problem. *Mathematics of Computation*, *52*, 495–508.

Dryja, M., & Widlund, O. B. (1989). Some domain decomposition algorithms for elliptic problems. In L. Hayes & D. Kincaid (Eds.), *Iterative methods for large linear systems* (pp. 273–291). San Diego, CA: Academic Press.

Franca, L. P., & Hughes, T. J. R. (1993). Convergence analysis of Galerkin least-squares methods for advective-diffusive forms of the Stokes and incompressible Navier-Stokes equations. *Computer Methods Applied Mechanics Engineering*, *105*, 285–298.

Franca, L. P., & Stenberg, R. (1991). Error analysis of some Galerkin least-squares methods for elasticity equations. *SIAM Journal of Numerical Analysis*, *28*, 1680–1697.

Feraudi, F., & Pennati, V. (1997). Transporto del calore in fluidi incomprimibili: Un nuovo approccio numerico per problemi bidimensionali non stazionari. *L'Energia Elettrica*, *74*(4), 238–251.

Fortin, M., & Boivin, S. (1990). Iterative stabilization of bilinear velocity-constant pressure element. *International Journal for Numerical Methods in Fluids*, *10*, 1680–1697.

Gervasio, P., & Saleri, F. (2006). Algebraic fractional step schemes for time-dependent incompressible Navier-Stokes equations. *Journal of Scientific Computing*, *27*(1–3), 257–269.

Guermond, J. L., & Quartapelle, L. (1998). On stability and convergence of projection methods based on pressure Poisson equation. *International Journal for Numerical Methods in Fluids*, *26*, 1039–1053.

Han, Z., Zhou, D., & Tu, J. (2013). Laminar flow patterns around three side-by-side arranged circular cylinders using semi implicit three step Taylor characteristic based split (3-Tcbs) algorithm. *Engineering Application Computational Fluid Mechanics*, *7*(1), 1–12.

Hookey, N. A., & Baliga, B. R. (1998). Evaluation and enhancements of some control volume finite-element methods-part 2. Incompressible fluid flow problems. *Numerical Heat Transfer*, *14*, 273–293.

Hughes, T. J. R., Franca, L. P., & Balestra, M. (1986). A new finite element formulation for computational fluids dynamics: V. Circumventing the Babuska-Brezzi condition: A stable Petrov- Galerkin formulation of the Stokes problem accomodating equal-order interpolations. *Computer Methods in Applied Mechanics Engineering*, *59*, 85–89.

Joe, B. (1991). GEOMPACK: A software package for the generation of meshes using geometric algorithms. *Advances in Engineering Software and Workstations*, *13*(5–6), 325–331.

Kengni Jotsa, A. C. (2010). *A new method for elliptic problems in CFD resembling the discontinuous FE approach*. Proceedings MASCOT 2010 Special Session, IMACS/ISGG, IMACS Series in Computational and Applied Mathematics, ULPGC; Las Palmas de Gran Canaria, Spain (pp. 219–228).

Kengni Jotsa, A. C. (2012). *Solution of the 2D Navier-Stokes Equations by a new FE fractional step method* (PhD thesis, Università Degli Studi Dell'Insubria Sede di Como, Italy). Retrieved from http://insubriaspace.cilea.it/handle/10277/477.

Kengni Jotsa, A. C., & Pennati, V. A. (2013). *Solution of 2D convection-diffusion transient problems by a fractional step FE method*. MASCOT11 Proceedings, IMACS Series in Computational and Applied Mathematics 17, IMACS, Rome (pp. 141–150).

Kim, J., & Moin, P. (1985). Application of fractional-step method to incompressible Navier-Stokes equations. *Journal of Computational Physics*, *59*, 308–323.

Kumar, D. S., Dass, A. K., & Dewan, A. (2010). A multigrid accelerate code on graded Cartesian meshes for 2D time dependent incompressible viscous flows. *Engineering Applications of Computational Fluid Mechanics*, *4*(1), 71–90.

Kumar, D. S., Kumar, K. S., & Kumar Das, M. (2009). A fine grid solution for a lid-driven cavity flow using a multigrid method. *Engineering Applications of Computational Fluid Mechanics*, *3*(3), 336–354.

Malan, A. G., Lewis, R.W., & Nithiarasu, P. (2002). An improved unsteady, unstructured, artificial compressibility, finite volume scheme for viscous incompressible flows: Part II. Application. *International Journal for Numerical Methods in Engineering*, *54*, 715–729.

Naga, A., & Zhang, Z. (2004). A posteriori error estimates based on the polynomial preserving recovery. *SIAM Journal of Numerical Analysis*, *42*, 1780–1800.

Pai, S. A., Prakash, P., & Patnaik, B. S. V. (2013). Numerical simulation of chaotic mixing in lid drive cavity: effect of passive plug. *Engineering Applications of Computational Fluid Mechanics*, *7*(3), 406–418.

Patankar, S. V. (1980). *Numerical heat transfer and fluid flow*. New York: Hemisphere.

Pironneau, O. (1982). On the transport-diffusion algorithm and its applications to the Navier-Stokes equations. *Numerische Mathematik*, *38*, 309–332.

Plana Fattori, A., Chantoiseau, E., Doursat, C., & Flick, D. (2013). Two-way coupling of fluid-flow, heat transfer and product transformation during heat treatment of starch suspension inside tubular exchanger. *Engineering Applications of Computational Fluid Mechanics*, *7*(3), 334–345.

Quarteroni, A., & Valli, A. (1999). *Domain decomposition methods for partial differential equations*. Oxford: Oxford Science Publications.

Shih, T. M., & Tan, C. H. (1989). Effects of grid staggering on numerical schemes. *International Journal for Numerical Methods of Fluids*, *9*, 193–212.

Shirokoff, D., & Rosales, R. R. (2011). An efficient method for the incompressible Navier-Stokes equations on irregular domains with no-slip boundary conditions, high order up to the boundary. *Journal of Computational Physics*, *230*, 8619–8646.

Silvester, P. J., & Kechkar, N. (1990). Stabilized bilinear-constant velocity pressure finite elements for the conjugate gradient solution of the Stokes problem. *Computer Methods in Applied Mechanics Engineering*, *79*, 71–86.

Stickland, M., Fabre, S., Scanlon, T., Oldroyd, A., Mickelson, T., & Astrup, P. (2013). CFD techniques for estimating flow distorsion effects on lidar measurements when made in complex flow fields. *Engineering Applications of Computational Fluid Mechanics*, *7*(3), 324–333.

Sun, X., Zhang, J. Z., & Ren, X. L. (2012). Characteristic based split (CBS) finite element method for incompressible viscous flow with moving boundaries. *Engineering Applications of Computational Fluid Mechanics*, *6*(3), 461–474.

Tritthart, M., & Gutknecht, D. (2007). Three dimensional simulation of free-surface flows using polyhedral finite volumes. *Engineering Applications of Computational Fluid Mechanics*, *1*(1), 1–14.

Van Doormal, J. P., & Raithby, G. D. (1984). Enhancements of the SIMPLE metodh for predicting incompressible fluid flows. *Numerical Heat Transfer*, *7*, 147–163.

Vrahliotis, S., Pappou, T., & Tsangaris, S. (2012). Artificial compressibility 3D Navier-Stokes solver for unsteady incompressible flows with hybrid grids. *Engineering Applications of Computational Fluid Mechanics*, *6*(2), 248–270.

Zang, Y., Street, R. L., & Koseff, J. R. (1994). A non-staggered grid, fractional step method for time-dependent incompressible Navier-Stokes equations in curvilinear coordinates. *Journal of Computational Physics*, *114*, 18–33.